

Posterior Distribution-assisted Evolutionary Dynamic Optimization as an Online Calibrator for Complex Social Simulations

Peng Yang, *Senior Member, IEEE*, Zhenhua Yang, Boquan Jiang, Chenkai Wang, Ke Tang, *Fellow, IEEE*, and Xin Yao, *Fellow, IEEE*

Abstract—The calibration of simulators for complex social systems aims to identify the optimal parameter that drives the output of the simulator best matching the target data observed from the system. As many social systems may change internally over time, calibration naturally becomes an online task, requiring parameters to be updated continuously to maintain the simulator’s fidelity. In this work, the online setting is first formulated as a dynamic optimization problem (DOP), requiring the search for a sequence of optimal parameters that fit the simulator to real system changes. However, in contrast to traditional DOP formulations, online calibration explicitly incorporates the observational data as the driver of environmental dynamics. Due to this fundamental difference, existing Evolutionary Dynamic Optimization (EDO) methods, despite being extensively studied for black-box DOPs, are ill-equipped to handle such a scenario. As a result, online calibration problems constitute a new set of challenging DOPs. Here, we propose to explicitly learn the posterior distributions of the parameters and the observational data, thereby facilitating both change detection and environmental adaptation of existing EDOs for this scenario. We thus present a pretrained posterior model for implementation, and fine-tune it during the optimization. Extensive tests on both economic and financial simulators verify that the posterior distribution strongly promotes EDOs in such DOPs widely existed in social science.

Index Terms—Evolutionary Dynamic Optimization, Online Data-driven Optimization, Complex Social Systems.

I. INTRODUCTION

MANY academic studies rely on computational simulations of complex social systems, e.g., economics [1], [2], finance [3], [4], and disease transmission [5]. Despite that physical mechanisms within social systems can be simulated accurately, varied sources of uncertainty, mostly related to human behaviors, cannot be precisely modeled and lack ground truth. Consequently, these uncertainties are usually described by the parameterized computational modules of the simulators to reflect a range of possibilities. Normally, to keep the simulation fidelity, the simulators are asked to replicate the observed data of a specific event of interest before being used [6], [7]. How to identify the optimal parameter of a given simulator for a specific event of the studied social system? This problem is called calibration in the literature [8], [9].

Peng Yang, Zhenhua Yang, Boquan Jiang, Chenkai Wang, and Ke Tang (*corresponding author*) are with the Guangdong Provincial Key Laboratory of Brain-Inspired Intelligent Computation, Southern University of Science and Technology, Shenzhen 518055, China. Peng Yang, Zhenhua Yang, Boquan Jiang, and Ke Tang are also with the Department of Computer Science and Engineering, and Peng Yang and Chenkai Wang are also with the Department of Statistics and Data Science. Zhenhua Yang is also with Zhongguancun Academy, Beijing 100094, China. (e-mail: {yangp, tangk3}@sustech.edu.cn; {yangzh2022, 12332460, wangck2022}@mail.sustech.edu.cn).

Xin Yao is with the School of Data Science, Lingnan University, Hong Kong SAR, China (e-mail: xinyao@ln.edu.hk).

Formally, let the observed data from the complex social system be $\{\hat{s}_t\}_{t=1}^T$, where $T \in \mathbb{N}^+$ indicates the total observation time steps, and $\hat{s}_t \in \mathbb{R}^{L \times m}$ is a m -variable data at the t -th observation time step with an observation window size of $L \in \mathbb{N}^+$. Given a parameterized simulator $M(\theta)$ with the parameter $\theta \in \mathbb{R}^d$, it can generate simulated time series data for any $T' > T$ observation time steps, denoted as $M(\theta, 1, T') = \{s_t\}_{t=1}^{T'}$, where $s_t \in \mathbb{R}^{L \times m}$. The calibration problem aims to find the optimal parameter θ^* that minimizes the discrepancy $D(\cdot)$ between the T -length observed and simulated data, formalized as $\theta^* = \arg \min_{\theta} D(\{\hat{s}_t\}_{t=1}^T, M(\theta, 1, T) = \{s_t\}_{t=1}^T)$. Intuitively, the calibration mainly works for replicating the historical social events ($t \leq T$) with a simulator for explaining what has happened previously, which is important for studying social systems [1]. Note that, this does not mean that the future observational data $\{\hat{s}_t\}_{t=T+1}^{T'}$ can be predicted by the simulator calibrated with data $\{\hat{s}_t\}_{t=1}^T$, unless the target system keeps unchanged within the interval of $1 \leq t \leq T'$, which hardly holds for social systems unless T' is close enough to T . Hence, the calibration problem does not take generalization issues into consideration, but aims to fit the simulated time series data to the observed trajectory¹. Since the simulator is often a software program and thus non-derivative, Evolutionary Algorithms (EAs) as powerful black-box optimization tools are usually adopted [10], [11].

In real-world applications, the target system often changes internally at an unknown timing, e.g., institutional investors may shift their strategies rapidly in financial markets [12]. Despite recent efforts on offline calibrating the changed systems using historical data [13]–[16], few research trials have been made in online scenarios where the data is continuously generated and observed. As a result, the optimal parameter of the simulator should be time-varying. Intuitively, this problem can be formulated as a Dynamic Optimization Problem (DOP), which aims to identify a sequence of optimal parameters that minimize the discrepancy between observed and simulated data whenever a change occurs in the target system [17]. To address DOPs, Evolutionary Dynamic Optimization (EDO) methods have been extensively studied [18], [19]. EDO methods are built upon the iterative search framework of EAs, aiming to detect environmental changes during the iterations [20], [21] and adapt to the new environment by managing and guiding the population [22]–[25].

However, while existing research on DOPs addresses continuously changing environments, those problem definitions

¹In this case, element-wise distances (e.g., Mean Squared Error) are often adopted as $D(\cdot)$ instead of distributional distances, for better measuring the similarity of two sequences of data.

rarely consider the underlying causes of such changes as online data. Therefore, although existing EDO methods can be applied to online calibration problems, their performance may be suboptimal. This is primarily due to two aspects:

1) *Change Detection*: Despite that the internal changes of a system can disrupt the objective function $D(\{\hat{s}_t\}_{t=1}^T, \{s_t\}_{t=1}^T)$ value, this value is also continuously changed since the observed data keeps coming in as T increases. This imposes a great challenge on existing EDOs, which detect environmental changes primarily based on the variations of objective function values. That is, traditional change detection strategies of EDOs cannot accurately distinguish "false changes" (evaluation error accumulations) from the real system changes.

2) *Environmental Adaptation*: According to the objective $D(\{\hat{s}_t\}_{t=1}^T, \{s_t\}_{t=1}^T)$, the environment of search space is directly defined by data $\{\hat{s}_t\}_{t=1}^T$. Given that real systems and simulators typically exhibit non-linear mappings from parameters to data, it is challenging to make assumptions about change patterns within the parameter space (e.g., smooth moving peaks [26] or periodic changes [27]) and explicitly model them, as is common in traditional EDO methods.

Intuitively, the above analysis implies that the challenges of applying EDOs to the online calibration problems lie in the gap between the traditional parameter space and the newly introduced data space. This paper proposes to address them by modeling a posterior distribution $p(\theta|\{\hat{s}_t\}_{t=1}^T)$ between the data and parameters, i.e., measuring the conditional probability of which parameter is more likely to be optimal given the observed data. More specifically, in the change detection phase, the posterior helps the detection resistant to the evaluation error accumulations, by focusing on the distributional changes of the incoming data, which are more likely to be caused by the internal changes of the real system. In the environmental adaptation phase, the posterior can serve as a computationally cheap surrogate for efficiently identifying the most promising areas in the parameter space regarding to the current observed data, without the calls of real evaluation functions.

To implement this, this paper learns the posterior distribution with a neural network-based masked autoregressive flow model [28], which takes the observed time series data $\{\hat{s}_t\}_{t=1}^T$ and a d -dimensional Gaussian distributional randomized vector as the inputs and outputs the predicted d -dimensional parameter θ and its posterior probability $p(\theta|\{\hat{s}_t\}_{t=1}^T)$. In this manner, the bridge between the parameter space and the data space is built. We train the neural network in an offline manner using a large volume of prepared pairs of parameters and their corresponding simulated data. During online calibration, i.e., the dynamic optimization process, the network is fine-tuned to better fit the observed data.

To assess how the proposed framework helps facilitate EDOs in the underlying DOP of online calibration, we conducted extensive experiments on both economic and finance simulators, covering a total of 18 synthetic instances with different frequencies of changes and lengths of incoming data. The results demonstrate that the proposed posterior distribution-assisted EDO significantly outperforms traditional EDOs in terms of solution quality and convergence. The ablations of the posterior distribution in both change detection

phase and the environmental adaptation phase also strongly verify its contributions to the performance.

The reminder of this paper is as follows. Section II reviews related work of simulator calibration and traditional EDOs. Section III formulates the online calibration problem and analyzes its differences to the definition of traditional DOPs. Section IV presents the proposed method in details. Section V describes the general experimental setups. Sections VI and VII report the results on two different simulators, respectively. Finally, Section VIII concludes this paper.

II. RELATED WORKS

A. Calibration of the Simulators

Calibrating simulators is widely present across various domains, e.g., finance [13], climate [16], and transportation [29]. According to the application requirements, calibration methods can be broadly divided into two categories: point estimation and distribution estimation. Distribution estimation aims to identify the optimal probabilistic distribution of the parameters given the observed data. Representative approaches include classical methods such as Simulated Maximum Likelihood [30], Approximate Bayesian Computation [31], and their neural network-based variants [28], [32], [33].

In contrast, point estimation aims to search for the optimal parameter by minimizing the discrepancy between the simulated and observed data. Several studies have focused explicitly on how to measure the discrepancy between time series data, aiming to better capture temporal dependencies, thereby improving the accuracy of calibration. Representative approaches include the element-wise distances (e.g., Mean Squared Error, and Simulated Moments) [9], [34], [35], and distributional discrepancies like the Wasserstein distance [36] and the Kolmogorov–Smirnov test [37]. Nevertheless, element-wise distances show significant superiority over distributional distances, since the simulator is expected to replicate element-wise the same time series data of the specific real event.

Considering that the calibration typically involves complex nonlinear systems, where the resulting objective functions are often non-differentiable and nonconvex, several studies have investigated EAs [13], [38], [39] and more recent surrogate-assisted approaches [37], [40] to improve the efficiency of the calibration process. In contrast to the online setting considered in this paper, most existing works can essentially be regarded as static optimization problems, which aims to identify a single solution for the on-hand observed data.

In recent years, some studies have attempted to address dynamic calibration, aiming to search a sequence of optimal parameters, instead of a single one. For example, in [13], [14], they find time-varying parameters with minimal discrepancy to the historical observed data. However, they do not address the online data stream scenarios and instead rely on completely collected observed data.

Others have considered the setting of online calibration, where observed data arrive continuously and different segments of the time series data may correspond to different optimal parameters of the simulator. For example, Carrassi et

al. [16] applied data assimilation techniques in the geosciences to sequentially update parameters or states by combining model outputs with new observations in real time. Zhu et al. [41] proposed a dynamic calibration framework for opinion dynamics models in the social sciences, integrating genetic algorithms with particle filters to adapt model parameters to successive observations. Zhang et al. [42] studied dynamic toll pricing within dynamic traffic assignment systems, applying online calibration to adjust traffic flow parameters under real-time conditions. These methods do not explicitly perform change detection, all assuming that every newly arrived observed data necessarily reflects a change of the real system. Unfortunately, this assumption does not align with real dynamics of many social systems, where the timing of changes is unknown.

B. Evolutionary Dynamic Optimization

In the literature, EDO is a class of methods that mostly relates to our problem setting, which explicitly addresses unknown changes and non-differentiable objective functions. EDO methods are built upon the iterative search framework of EAs, aiming to not only detect environmental changes but also rapidly adapt to new environments during the optimization process.

In traditional EDO, the environment is often considered as the parameter space, and thus the changes are detected by monitoring the changes in the objective function values [20], [21]. Specifically, detector-based detection places detectors at fixed locations in the parameter space to continuously monitor their objective values and identify environmental changes [43]. And fitness-based detection tracks the fitness values of selected individuals (e.g., the best ones) during the optimization process and triggers change detection if no improvement is observed within a predefined number of iterations [13], [44].

The environmental adaptation is another key component of EDO, aiming to quickly recover the search capability by redistributing the population once an environmental change is detected. Typical strategies include re-initializing part or all of the population to increase the diversity [20], intensifying mutation or adjusting control parameters to broaden the search areas [45], and leveraging historical information through explicit archives of good solutions to accelerate adaptation [25]. More recently, prediction-based approaches have also been proposed, which attempt to anticipate future environmental changes and proactively guide the search process [46]–[49]. Recently, deep generative models, such as diffusion models [50] and Recurrent Neural Networks (RNNs) [51], have also been introduced to capture complex environmental dynamics. For example, the neural network-based information transfer (NNIT) method re-evaluates the objective function values of past search trajectories in the current environment to train neural models, thereby enabling knowledge transfer and facilitating the generation of new candidate solutions [46].

In addition, to support the two major components mentioned above, techniques such as convergence detection and population division and management have also been investigated. Among them, convergence detection is used to determine

whether the population has already converged, so that the iterations can be terminated early to save computational cost [52]; it also serves to identify premature convergence, in which case population diversity can be increased to restore exploration capability [53]. Population division and management divides the population into multiple subgroups that perform independent or cooperative searches, helping maintain diversity and improve adaptability in dynamic environments [17], [54].

To our best knowledge, no EDO method has been investigated in the online calibration problems, where the changes are uniquely caused by the incoming online data. In the next section, we rigorously identify the key challenges that traditional EDOs face in this context, motivating the further designs of our Posterior Distribution-assisted EDO.

III. PROBLEM FORMULATION AND CHALLENGES

In this section, we first formalize the online calibration as a DOP, which aims to clearly characterize how simulator parameters dynamically adjust in response to sequentially arriving observed data under unknown system internal changes. On this basis, we analyze why existing EDOs are not suitable for the online calibration.

Consider that the observed data $\{\hat{s}_t\}_{t=1}^T, T \in \mathbb{N}^+$ comes in step-by-step, with a observation window of L at each time step t . And the current time step is denoted as $t = T_c, 1 \leq T_c \leq T$. Suppose the system undergoes K internal changes, and each i -th change happens at time $\tilde{T}_{\tau_i}, i = 0, \dots, K - 1$, with $\tilde{T}_{\tau_0} = 1$. These unknown change points naturally divide the online calibration problem into K consecutive subproblems. The objective of the online calibrator is to search for the optimal parameter sequence $\{\theta_i^*\}_{i=0}^{K-1}$ of the simulator within $t \in [1, T]$, where θ_i^* denotes the optimal solution to the i -th subproblem within $t \in [\tilde{T}_{\tau_{i-1}}, \tilde{T}_{\tau_i}]$, thus the objective function can be formulated as:

$$\{\theta_i^*\}_{i=1}^K = \underset{\theta}{\operatorname{argmin}} D\left(\{\hat{s}_t\}_{t=\tilde{T}_{\tau_{i-1}}}^{T_c}, M(\theta, \tilde{T}_{\tau_{i-1}}, T_c)\right), \quad (1)$$

for $i = 1, \dots, K$,

where $M(\theta, \tilde{T}_{\tau_{i-1}}, T_c) = \{s_t\}_{t=\tilde{T}_{\tau_{i-1}}}^{T_c}$ indicates that the simulator continuously generates data as the current time T_c goes by. Accordingly, the current i -th subproblem is based on the observed data $\{\hat{s}_t\}_{t=\tilde{T}_{\tau_{i-1}}}^{T_c}$, starting from the most recent change point $\tilde{T}_{\tau_{i-1}}$ to T_c , and continues until the next change time \tilde{T}_{τ_i} . For the calibration in each i -th subproblem, the optimization is guided by the discrepancy between the simulated data $\{s_t\}_{t=\tilde{T}_{\tau_{i-1}}}^{T_c}$ and the observed data $\{\hat{s}_t\}_{t=\tilde{T}_{\tau_{i-1}}}^{T_c}$.

To better understand the dynamics of the above problem, we first borrow the simplified formulation of traditional DOPs from [22], described as follow:

$$\{\theta_i^*\}_{i=1}^K = \underset{\theta}{\operatorname{argmin}} f(\theta, \alpha(i)), \quad \text{for } i = 1, 2, \dots, K, \quad (2)$$

where the objective function f undergoes K changes, yielding K subproblems, and the environment of the i -th subproblem is determined by $\alpha(i)$, i.e., a certain configuration of the objective function.

Accordingly, we present a simplified form of Eq.(1) as:

$$\{\boldsymbol{\theta}_i^*\}_{i=1}^K = \underset{\boldsymbol{\theta}}{\operatorname{argmin}} D(\boldsymbol{\theta}, \beta(i, \{\hat{s}_t\}, T_c)), \text{ for } i = 1, \dots, K. \quad (3)$$

The simplification is made by separating the parameter $\boldsymbol{\theta}$ from all possible dynamics in Eq.(1). Specifically, $\beta(i, \{\hat{s}_t\}, T_c)$ is devised to include all the dynamics of Eq.(1) caused by the incoming data $\{\hat{s}_t\}_{t=\tilde{T}_{\tau_{i-1}}}^{T_c}$. Among them, i comes from the last change point $t = \tilde{T}_{\tau_{i-1}}$, $\{\hat{s}_t\}$ indicates the incoming time series data, and T_c denotes the current observation time $t = T_c$. By comparing Eqs.(2)-(3), it is clear to distinguish them.

First, although both problems have unknown changes that need to be detected, the difficulty of change detection is different. For Eq.(2), the environment within each i -th subproblem is static since the internal changes are solely determined by $\alpha(i)$ with the last change point index i . Hence, the environmental changes can be accurately detected by monitoring the changes of the objective function values. For Eq.(3), the environment of each i -th subproblem is dynamic, as it is additionally influenced by the incoming data $\{\hat{s}_t\}$ and the current observation time $t = T_c$. On one hand, the internal changes of the target system will cause substantial distributional shifts of the incoming data $\{\hat{s}_t\}$, which thus can be easily monitored through the value changes of Eq.(1). On the other hand, the increasing T_c can also lead to varied objective function values that do not necessarily correspond to internal changes, as it accumulates the discrepancy errors between the observed and simulated data over time. Since there is a lack of a clear relationship between the data changes and the objective function values, existing change detection methods may be ineffective to tell the “false changes” of evaluation error accumulations from the real distributional changes.

Second, after environmental changes, the search process should adapt to the new environment to achieve faster convergence. Existing EDOs typically assume that the environmental change controlling function $\alpha(i)$ follows specific patterns, such as smooth moving peaks [26] and periodic variations [27]. In this regard, they adapt to new environments by modeling the changes in the parameter space, or explicitly archiving promising regions for future use. However, as shown in Eq.(1), the environmental changes of online calibration depend directly on the continuously arriving observed data. Due to the nonlinear relationship between the data and the parameters, the changes exhibit complex patterns that may be far beyond those assumptions, making it difficult for existing EDOs to adapt the population to such changes effectively.

In summary, the online calibration suffers from more complex causes of changes than traditional black-box DOPs settings. This challenges both change detection and environment adaptation of existing EDOs. And the above challenges can be owed to the unknown yet non-linear relationship between the data and the parameters.

IV. THE PROPOSED METHOD

This work proposes to address the above challenge by explicitly estimating the non-linear relationship between data and parameters as a posterior distribution. In this section, we

first describe how a posterior distribution can assist the change detection and environment adaptation phases. After that, we detail how to learn the posterior using a pretrained neural network-based flow model and finetune it during optimization. Last, the overall framework of the posterior distribution-assisted EDO is presented.

A. Change Detection and Environment Adaptation

Let the posterior distribution between the observed data sequence $\{\hat{s}_t\}$ and the parameters $\boldsymbol{\theta}$ be $p_\phi(\boldsymbol{\theta}|\{\hat{s}_t\})$, which represents the conditional probability of each parameter being optimal given the observed data $\{\hat{s}_t\}$. It can facilitate both change detection and environment adaptation in online calibration. In the change detection phase, $p_\phi(\boldsymbol{\theta}|\{\hat{s}_t\})$ can eliminate the “false changes” situation caused by T_c . Specifically, as long as the internal changes did not occur, the incoming data will follow the same generative distribution of the unchanged observed system. In this regard, the posterior distribution should also remain unchanged, regardless of whether the observed data is increasing. Contrarily, if $p_\phi(\boldsymbol{\theta}|\{\hat{s}_t\})$ changes, it signifies an internal change of the observed system. In the environmental adaptation phase, since $p_\phi(\boldsymbol{\theta}|\{\hat{s}_t\})$ can measure the probability of each $\boldsymbol{\theta}$ being optimal given the environment defined by $\{\hat{s}_t\}$, we can directly sample parameters with high probability therefrom and take those parameters as the adapted population in the new environment.

Algorithm 1 describes the change detection procedure when the posterior distribution is available. More specifically, change detection requires determining whether the system has changed at $t = T_c$ based on the most recently observed data $\{\hat{s}_t\}_{t=\tilde{T}_{\tau_{i-1}}}^{T_c}$ since the last detected change time $T_{\tau_{i-1}}$. For that purpose, we first take $\{\hat{s}_t\}_{t=\tilde{T}_{\tau_{i-1}}}^{T_c-1}$ and \hat{s}_{T_c} as conditions into the posterior distribution to obtain $p_\phi(\boldsymbol{\theta}|\{\hat{s}_t\}_{t=\tilde{T}_{\tau_{i-1}}}^{T_c-1})$ and $p_\phi(\boldsymbol{\theta}|\hat{s}_{T_c})$, respectively. After that, the discrepancy between the two parameter distributions is quantified with the Kullback–Leibler (KL) divergence D_{KL} , as follows:

$$D_{KL} = \sum_{n=1}^N p_\phi(\boldsymbol{\theta}_n|\hat{s}_{T_c}) \log \frac{p_\phi(\boldsymbol{\theta}_n|\hat{s}_{T_c})}{p_\phi(\boldsymbol{\theta}_n|\{\hat{s}_t\}_{t=\tilde{T}_{\tau_{i-1}}}^{T_c-1})}. \quad (4)$$

Eq.(4) is a Monte-Carlo approximation of the KL divergence, which can be varied with N random samples. Here, a threshold ε is set to regulate the sensitivity of change detection. If $D_{KL} < \varepsilon$, indicating no internal change has occurred, the online calibration process continues to progress to the next time $T_c \leftarrow T_c + 1$. Otherwise, it indicates that the newly received data \hat{s}_{T_c} has distributionally shifted, and the current time is recorded as the next changed observation time $T_{\tau_i} \leftarrow T_c$, which then triggers the environment adaptation process.

The environment adaptation process is to enhance the exploration ability in the dynamic environment. Specifically, the original population (at $t = T_c - 1$) is replaced by the adapted population to continue the search in the new environment (starting at $t = T_c$). The adapted population $\boldsymbol{\Theta} = \{\boldsymbol{\theta}_j\}_{j=1}^\lambda$ is constructed by sampling from the posterior distribution $p_\phi(\boldsymbol{\theta}|\hat{s}_{T_c})$, conditioned on the current observed

Algorithm 1 ChangeDetection($p_\phi, \{\hat{s}_t\}_{t=T_{\tau_{i-1}}}^{T_c}, \varepsilon$)

Input: Posterior distribution p_ϕ ; observed data since last change point $\{\hat{s}_t\}_{t=T_{\tau_{i-1}}}^{T_c}$; threshold ε .

Output: Change flag $flag$

- 1: Initialize: $flag \leftarrow \text{false}$
- 2: Compute D_{KL} between $p_\phi(\boldsymbol{\theta} | \{\hat{s}_t\}_{t=T_{\tau_{i-1}}}^{T_c-1})$ and $p_\phi(\boldsymbol{\theta} | \hat{s}_{T_c})$ using Eq. (4);
- 3: **if** $D_{KL} \geq \varepsilon$ **then**
- 4: $flag \leftarrow \text{true}$.
- 5: **end if**

Algorithm 2 Adaptation($p_\phi, \hat{s}_{T_c}, \lambda$)

Input: Posterior distribution p_ϕ , the last observed data \hat{s}_{T_c} , population size λ .

Output: Adapted population $\Theta = \{\boldsymbol{\theta}_j\}_{j=1}^\lambda$.

- 1: Draw samples $\{\boldsymbol{\theta}_n\}_{n=1}^N \sim p_\phi(\boldsymbol{\theta} | \hat{s}_{T_c})$;
- 2: Set $\Theta \leftarrow \{\boldsymbol{\theta}_1\}$, $\boldsymbol{\theta}_1 \sim \text{Uniform}(\{\boldsymbol{\theta}_n\}_{n=1}^N)$;
- 3: **for** $j = 2$ to λ **do**
- 4: $\boldsymbol{\theta}_j = \text{argmax}_{\boldsymbol{\theta} \in \{\boldsymbol{\theta}_n\}_{n=1}^N \setminus \Theta} \sum_{\boldsymbol{\theta}' \in \Theta} \|\boldsymbol{\theta} - \boldsymbol{\theta}'\|_2$;
- 5: $\Theta \leftarrow \Theta \cup \{\boldsymbol{\theta}_j\}$;
- 6: **end for**

data \hat{s}_{T_c} . To prevent the initialized population from being overly concentrated in the parameter space, we first draw a candidate set of parameters $\{\boldsymbol{\theta}_n\}_{n=1}^N$ from $p_\phi(\boldsymbol{\theta} | \hat{s}_{T_c})$, and then select λ individuals that maximize the pairwise Euclidean distances in the parameter space. The complete environment adaptation procedure is summarized in Algorithm 2.

B. Flow-based Posterior Distribution Estimator

Leveraging the strong capability of flow-based models in fitting complex distributions, we employ a neural network based masked autoregressive flow (MAF) to model the posterior distribution $p_\phi(\boldsymbol{\theta} | \{\hat{s}_t\})$ [28]. To this end, the MAF defines a conditional invertible transformation f_ϕ , where ϕ denotes the neural network parameters, that transforms samples \mathbf{z} from a simple base distribution into the parameters $\boldsymbol{\theta}$ under the conditioning of the observed data $\{\hat{s}_t\}$, i.e., $\boldsymbol{\theta} = f_\phi(\mathbf{z}; \{\hat{s}_t\})$, $\mathbf{z} \sim \mathcal{N}(\mathbf{0}, \mathbf{I})$ denotes the latent variable from the multidimensional standard Gaussian distribution.

In the implementation, f_ϕ consists of 10 layers: five masked autoregressive affine transformation layers interleaved with five random permutation layers. Each masked autoregressive affine transformation layer takes the parameter vector $\boldsymbol{\theta}^{(l-1)}$ from the $(l-1)$ -th layer and the conditioning data $\{\hat{s}_t\}$ as input, and outputs the transformed parameter vector $\boldsymbol{\theta}^{(l)}$ for the next random permutation layer, which reorders the dimensions of $\boldsymbol{\theta}^{(l)}$ to alter the autoregressive dependency structure. The MAF starts from the latent variable $\boldsymbol{\theta}^{(0)} = \mathbf{z}$ and sequentially transforms it through five layers to obtain the final parameter $\boldsymbol{\theta}$. Formally, for each dimension i of the $\boldsymbol{\theta}^{(l)}$,

$$\boldsymbol{\theta}_i^{(l)} = \mu_i^{(l)}(\boldsymbol{\theta}_{1:i-1}^{(l-1)}, \{\hat{s}_t\}) + \sigma_i^{(l)}(\boldsymbol{\theta}_{1:i-1}^{(l-1)}, \{\hat{s}_t\}) \cdot \boldsymbol{\theta}_i^{(l-1)},$$

where $\mu_i^{(l)}(\cdot)$ and $\sigma_i^{(l)}(\cdot)$ are autoregressive functions implemented by masked multilayer perceptrons (MLPs). Each MLP

Algorithm 3 Training($p_\phi, \mathcal{D}, E_{max}$)

Input: posterior p_ϕ , Training dataset $\mathcal{D} = \{\langle \boldsymbol{\theta}_m, \{\hat{s}_t\}_m \rangle\}$, number of epochs without improvement E_{max} .

Output: posterior p_ϕ .

- 1: Initialize: $e \leftarrow 0, \phi, \eta, \mathcal{L}_{best} \leftarrow \infty$;
- 2: **while** $e < E_{max}$ **do**
- 3: **for** each mini-batch $\{\langle \boldsymbol{\theta}_m, \{\hat{s}_t\}_m \rangle\}_{m=1}^B$ from \mathcal{D} **do**
- 4: Compute loss $\mathcal{L}(\phi)$ using Eq. (6);
- 5: Update parameters $\phi \leftarrow \phi - \eta \nabla_\phi \mathcal{L}(\phi)$;
- 6: **end for**
- 7: **if** $\mathcal{L}(\phi) < \mathcal{L}_{best}$ **then**
- 8: $\mathcal{L}_{best} \leftarrow \mathcal{L}(\phi)$;
- 9: $e \leftarrow 0$;
- 10: **else**
- 11: $e \leftarrow e + 1$;
- 12: **end if**
- 13: **end while**

consists of two fully connected layers with 50 hidden units and ReLU activations. The conditioning data $\{\hat{s}_t\}$ are first mapped by a representation function $R(\cdot)$ into an embedded vector of dimensions k , i.e., $R(\{\hat{s}_t\}) \in \mathbb{R}^k$, which serves as an additional input to each autoregressive transformation to incorporate contextual information from the observed data. Therefore, the input dimension to each MLP is $d+k$, and the output dimension is d . In practice, we consider $R(\cdot)$ as the commonly adopted $k=9$ length-invariant summary statistics of time series data, i.e., the mean, median, variance, range, minimum, maximum, skewness, kurtosis, and interquartile range of a given $\{\hat{s}_t\}$.

During training, its inverse mapping f_ϕ^{-1} is applied to transform $\boldsymbol{\theta}$ back to \mathbf{z} , which allows the conditional log-likelihood to be computed as:

$$\log p_\phi(\boldsymbol{\theta} | \{\hat{s}_t\}) = \log p(\mathbf{z}) + \log \left| \det \left(\frac{\partial f_\phi^{-1}(\boldsymbol{\theta}; \{\hat{s}_t\})}{\partial \boldsymbol{\theta}} \right) \right|, \quad (5)$$

where $\det(\cdot)$ represents the Jacobian determinant of a matrix. Then, the overall training objective is to maximize this conditional log-likelihood over mini-batches of the dataset:

$$\mathcal{L}(\phi) = \frac{1}{B} \sum_{m=1}^B \log p_\phi(\boldsymbol{\theta}_m | \{\hat{s}_t\}_m), \quad (6)$$

where B denotes the batch size. Training is terminated early if the loss shows no improvement for E_{max} consecutive epochs, to prevent overfitting and reduce computational costs. The detailed algorithm for training the flow-based posterior on dataset \mathcal{D} is presented in Algorithm 3.

We obtain the posterioator before online calibration via a pretrning manner. This is because the mapping between the parameter space and the data space is deterministic once the simulator $M(\cdot)$ has been given. The dataset $\mathcal{D}_{pre} = \{\langle \boldsymbol{\theta}_m, \{\hat{s}_t\}_m \rangle\}_{m=1}^{|\mathcal{D}_{pre}|}$ for pretraining is constructed as follows. First, we sample $|\mathcal{D}_{pre}|$ parameters uniformly from the parameter space \mathcal{P} , that is, $\{\boldsymbol{\theta}_m\}_{m=1}^{|\mathcal{D}_{pre}|} \sim \mathcal{U}(\mathcal{P})$. For each $\boldsymbol{\theta}_m$, we choose the different start and end observation time T_m^{start} and

T_m^{end} , then run the simulator to generate the corresponding data $\{\mathbf{s}_t\}_m = M(\boldsymbol{\theta}_m, T_m^{\text{start}}, T_m^{\text{end}})$.

C. Optimization with Fine-tuning

During each observation period t , a data slide $\hat{\mathbf{s}}_t \in \mathbb{R}^{L \times m}$ is observed, with $m \in \mathbb{N}^+$ variables and an observation window size of $L \in \mathbb{N}^+$. According to Eq.(1), the objective at each $t = T_c$ is to minimize the discrepancy between the observed data $\{\hat{\mathbf{s}}_t\}_{t=T_{\tau_{i-1}}}^{T_c}$ and the simulated data $\{\mathbf{s}_t\}_{t=T_{\tau_{i-1}}}^{T_c}$:

$$\boldsymbol{\theta}_i^* = \operatorname{argmin}_{\boldsymbol{\theta}} D\left(\{\hat{\mathbf{s}}_t\}_{t=T_{\tau_{i-1}}}^{T_c}, M(\boldsymbol{\theta}, T_{\tau_{i-1}}, T_c) = \{\mathbf{s}_t\}_{t=T_{\tau_{i-1}}}^{T_c}\right). \quad (7)$$

Therefore, at each $t = T_c$, the optimization process is triggered to search the optimal parameter $\boldsymbol{\theta}^*$ based on the last population Θ for I_{\max} algorithm iterations. In general, any existing evolutionary operators can be employed to drive the search.

To implement the discrepancy metric, we consider the method of simulated moments [9], [34], i.e., a weighted mean squared error (MSE), between the summary statistics of the simulated data and the observed data:

$$\begin{aligned} & D\left(\{\hat{\mathbf{s}}_t\}_{t=T_{\tau_{i-1}}}^{T_c}, \{\mathbf{s}_t\}_{t=T_{\tau_{i-1}}}^{T_c}\right) \\ &= \frac{1}{k} \left\| R(\{\hat{\mathbf{s}}_t\}_{t=T_{\tau_{i-1}}}^{T_c}) - R(\{\mathbf{s}_t\}_{t=T_{\tau_{i-1}}}^{T_c}) \right\|_2^2. \end{aligned} \quad (8)$$

To further align the pretrained posterior p_ϕ with the underlying observed data, we collect the finetuning dataset \mathcal{D}_{fin} in parallel with the optimization process. That is, while the new population of λ individuals $\{\boldsymbol{\theta}_j\}_{j=1}^\lambda$ are generated iteratively, we simulate each of them from $t = T_{\tau_{i-1}}$ to T_c to obtain the simulated data, i.e., $\{\mathbf{s}_t\}_{t=T_{\tau_{i-1}}}^{T_c} = M(\boldsymbol{\theta}_j, T_{\tau_{i-1}}, T_c)$. And those pairwise tuples $\langle \boldsymbol{\theta}_j, \{\mathbf{s}_t\}_{t=T_{\tau_{i-1}}}^{T_c} \rangle$ are collected to form \mathcal{D}_{fin} . The size of the dataset is determined by the number of simulator runs performed during the optimization, normally $\lambda \cdot I_{\max}$. This joint procedure allows the posterior estimator to maintain both local adaptability and global consistency as the environment changes. The complete workflow is described in Algorithm 4.

D. The PosEDO Framework

Building upon the three components introduced in the previous section, we now present the complete PosEDO framework for online calibration.

As shown in Algorithm 5, the goal is to obtain a set of calibrated parameters $S = \{\boldsymbol{\theta}_i\}$ as T_c continuously increases, where each $\boldsymbol{\theta}_i$ is the best-found parameter within the observation period of $t \in [T_{\tau_{i-1}}, T_{\tau_i}]$. To this end, the overall framework is divided into two phases: offline pretraining and online calibration. First, the pretraining dataset \mathcal{D}_{pre} is used to train the posterior distribution p_ϕ before online calibration. In the online calibration phase, PosEDO solves Eq. (7) for each observation sequentially as T_c increases. Specifically, for each observed data $\hat{\mathbf{s}}_{T_c}$, PosEDO first evolves the population Θ with any qualified evolutionary algorithm for I_{\max} iterations, which also generates a new dataset \mathcal{D}_{fin} for finetuning p_ϕ . Then, based on the finetuned p_ϕ , the change detection module

Algorithm 4 Optimization($\Theta, I_{\max}, \lambda, T_{\tau_{i-1}}, T_c$)

Input: last population Θ ; maximum iterations I_{\max} ; population size λ ; last change point $T_{\tau_{i-1}}$; current time T_c .
Output: Best-found parameter $\boldsymbol{\theta}^*$; the last population Θ ; fine-tuning dataset \mathcal{D}_{fin} .

- 1: Initialize: $iter \leftarrow 1, \mathcal{D}_{fin} \leftarrow \emptyset$;
- 2: **while** $iter \leq I_{\max}$ **do**
- 3: **for** each individual $\boldsymbol{\theta}_j$ in the population Θ **do**
- 4: $\{\mathbf{s}_t\}_{t=T_{\tau_{i-1}}}^{T_c} \leftarrow M(\boldsymbol{\theta}_j, T_{\tau_{i-1}}, T_c)$;
- 5: Fitness evaluation using Eq.(8);
- 6: Store data $\mathcal{D}_{fin} \leftarrow \mathcal{D}_{fin} \cup \langle \boldsymbol{\theta}_j, \{\mathbf{s}_t\}_{t=T_{\tau_{i-1}}}^{T_c} \rangle$;
- 7: **end for**
- 8: Keep the best-found parameter as $\boldsymbol{\theta}^*$;
- 9: Update Θ using certain evolutionary operators;
- 10: $iter \leftarrow iter + 1$.
- 11: **end while**

works for identifying whether there is an internal change with the newly observed data. If so, the current time step T_c is recoded as a new change point, and the best-found individual is also archived as the calibrated parameter since the last change point. After that, the environmental adaptation module is evoked to obtain a population of λ new individuals that are highly likely to survive in the new environment (defined by the current observed data $\hat{\mathbf{s}}_{T_c}$) by guided sampling from p_ϕ . Subsequently, the last population before the current change point is omitted, and the new individuals are considered as Θ for further evolution. On the other hand, if the change detection module returns false, the best-found individual $\boldsymbol{\theta}^*$ from the current observation is recorded as the calibrated parameter since the last change point. Accordingly, the evolution for the current observation period $t = T_c$ is considered finished, and new data is observed, i.e., $T_c = T_c + 1$.

V. EXPERIMENTAL SETUP

The experimental setup includes the following aspects. First, two representative simulators from different domains are introduced to construct the experimental environment. Next, four compared algorithms are adopted as baselines by incorporating the typical change detection and environment adaptation. Finally, the detailed parameter configurations all algorithms used in the experiments are presented.

A. Simulators from Different Domains

To comprehensively evaluate PosEDO on the different online calibration tasks, we select two complex multi-agent based simulators from different domains: one from the economic field for modeling macro asset prices and the other from the financial field for modeling the market microstructure. Both simulators have been intensively studied in traditional static calibration works [9], [55]. They differ significantly in parameter dimensionality and internal behavioral complexity, thus forming diverse experimental environments.

Algorithm 5 Online Calibration Framework

Input: threshold ε , maximum iteration I_{max} , pretraining epoch E_{pre} , finetuning epoch E_{fin} , pretraining dataset D_{pre} .
Output: calibrated parameters S ; change points set T_τ .

Offline Pretraining Phase:

- 1: Initialize the p_ϕ ;
- 2: $p_\phi \leftarrow \text{Training}(p_\phi, \mathcal{D}_{pre}, E_{pre})$;

Online Calibration Phase:

- 1: Initialize: $S \leftarrow \emptyset$, $T_c \leftarrow 1$, $i \leftarrow 1$, $T_\tau \leftarrow \{T_c\}$;
- 2: Randomly initialize the population $\Theta = \{\theta_j\}_{j=1}^\lambda$;
- 3: **for** each observation \hat{s}_{T_c} at time T_c **do**
- 4: $\{\theta^*, \Theta, \mathcal{D}_{fin}\} \leftarrow \text{Optimization}(\Theta, I_{max}, \lambda, T_{\tau_{i-1}}, T_c)$;
- 5: $p_\phi \leftarrow \text{Training}(p_\phi, \mathcal{D}_{fin}, E_{fin})$;
- 6: **if** $T_c \neq T_{\tau_{i-1}}$ **then**
- 7: **if** $\text{ChangeDetection}(p_\phi, \{\hat{s}_t\}_{t=T_{\tau_{i-1}}}^{T_c}, \varepsilon)$ **then**
- 8: $T_\tau \leftarrow T_\tau \cup \{T_c\}$;
- 9: $S \leftarrow S \cup \{\theta_i^*\}$; $i \leftarrow i + 1$;
- 10: $\Theta \leftarrow \text{Adaptation}(p_\phi, \hat{s}_{T_c}, \lambda)$;
- 11: **else**
- 12: $\theta_i^* \leftarrow \theta^*$;
- 13: $T_c \leftarrow T_c + 1$;
- 14: **end if**
- 15: **end if**
- 16: **end for**

1) *The Brock and Hommes Model [2]:* This simulator captures price dynamics driven by heterogeneous expectations and is commonly used to study complex feedback mechanisms in economic systems. Although the model contains relatively few parameters, it exhibits strong nonlinear dynamics and even chaotic behaviors. In this work, we focus on calibrating two key parameters $[g_2, b_2]$ that substantially influence system stability, as they jointly determine the agents' trend-following intensity and bias in price expectations, with $g_2 \in [0.5, 1]$ and $b_2 \in [0, 1]$. Specifically, at each time step, the trend-following agents extrapolate the past price deviation with an intensity factor g_2 to predict the future price movement, while b_2 acts as a constant bias added to this expectation, directly shifting the aggregate demand curve. The motivation for choosing only two measurements is twofold. First, it highlights a typical low-dimensional yet behaviorally complex dynamic calibration problem. Second, it provides a clearer test of whether traditional EDO methods can effectively cope with a seemingly "simple" scenario, thereby highlighting the inherent difficulty of the online calibration. We construct 9 test instances with 3 different change frequencies, i.e., the number of change points K is 3, 5, or 8. Each instance contains a sequence of 30 observations, where each observation corresponds to a time series of size $L \times m = 50 \times 1$.

2) *The Preis-Golke-Paul-Schneid (PGPS) Model [56]:* The PGPS model is a multi-agent limit-order-book simulator widely used to model stock market interactions and price formation. The model simulates two types of agents: liquidity providers and liquidity takers. In the experiments, each type

consists of 125 trading agents that simulate the behavior of a realistic trading process. This model is governed by six key parameters: $\mathbf{w} = [\alpha, \mu, \delta, \Delta S, \lambda_0, C_\lambda]$, which control key aspects such as order price bias, response speed, and order submission mechanisms, with their ranges summarized in [57]. Specifically, α and μ represent the fixed probabilities for liquidity providers to submit limit orders and for liquidity takers to submit market orders, respectively. The parameter δ specifies the probability of cancelling an untraded order, while ΔS determines the increment size of the mean-reverting random walk that governs the agents' buy or sell direction. Finally, λ_0 and C_λ jointly calculate the time-variant order placement depth $\lambda(t)$, determining the price of limit orders relative to the best bid/ask prices based on current market imbalances. Compared to the Brock and Hommes model, the PGPS model exhibits higher dimensionality and stronger interaction complexity (prices are determined by agents' orders rather than their general beliefs), making it significantly more challenging for dynamic optimization algorithms. There are also 9 test instances obtained by combining 3, 4, and 5 parameter configurations with varying change frequencies, and each instance contains a sequence of 18 observations, where each observation corresponds to a time series of size $L \times m = 200 \times 1$.

B. Algorithms Setup

To thoroughly assess the effectiveness of the proposed online calibration method, we systematically compare it with several representative EDO methods from the perspectives of change detection and environment adaptation. The change detection strategies of these baseline methods are divided into two categories. The first is the detector-based detection (DBD) method, which deploys detectors at fixed locations to monitor fitness values, where a variation in fitness indicates a detected change [20]. The second is the fitness-based change detection (FBCD) method, which tracks the best fitness value over time and triggers change detection if no improvement is observed over a predefined number of generations [13].

Besides the above detection approaches, three different environment adaptation mechanisms from EDOs are utilized. These include random re-initialization of the population (Rand), which uniformly samples parameters from the search space to initialize the population. The explicit memory archive technique (Arch) is also employed to reuse historical elite solutions under the assumption that environmental changes are periodic [25]. In addition, neural network-based information transfer (NNIT) [46] as a representative of predictive transfer methods is utilized. In NNIT, neural models trained on past search trajectories, combined with information from new environment, facilitate the generation of new solutions.

The optimization method in PosEDO is compatible with both single-population and multi-population algorithms. Due to the multimodal nature of the calibration problem [38], multi-population algorithms provide more thorough exploration of the environment compared to single-population ones. Therefore, in the experiments, to more effectively explore and demonstrate how our method can be adapted to work

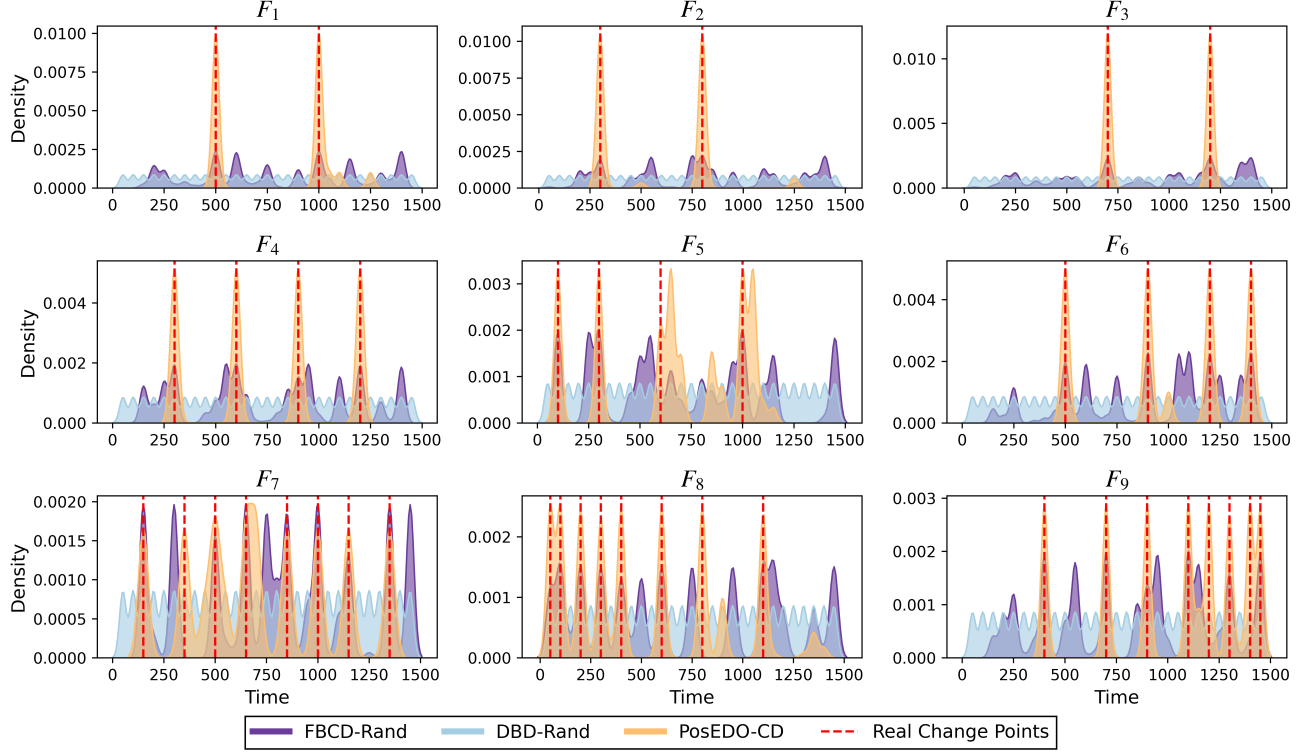


Fig. 1: Comparison of detection accuracy across 9 benchmark instances (F_1 – F_9) on the Brock–Hommes model. In each subplot, the red dashed lines indicate the ground-truth change points. The purple, blue, and orange curves represent the change detection probability densities of FBCD-Rand, DBD-Rand, and PosEDO-CD, respectively.

with more complex multi-population EDOs, all optimization methods of these algorithms are implemented on the adaptive multi-population framework with PSO (AMP/PSO) [58]. We modify AMP/PSO to explicitly incorporate change detection, while keeping the rest of the settings consistent with the original method. Therefore, all the compared algorithms are summarized as: a) our complete method using posterior-based change detection and environment adaptation (PosEDO). b) detector-based detection with random re-initialization (DBD-Rand); c) fitness-based change detection with random re-initialization (FBCD-Rand); d) fitness-based change detection with explicit archive-based adaptation (FBCD-Arch); e) fitness-based change detection with NNIT-based transfer (FBCD-NNIT); f) our posterior-based change detection with pretraining only, without fine-tuning (PosEDo-Pre); and g) our posterior-based change detection method with random re-initialization (PosEDo-CD). Among these algorithms, b)–e) correspond to traditional EDO-based baselines with different change detection and adaptation mechanisms, whereas f) and g) are ablation variants of the proposed PosEDO framework used to analyze the contributions of posterior pretraining, fine-tuning, and posterior-based change detection.

C. Performance Metrics

To evaluate the performance of different algorithms in the online calibration task, two metrics are employed in the experiments.

1) *Mean Calibration Error*: The mean calibration error (MCE) is used to quantify the overall accuracy of the online calibration process. It measures the average calibration error across all subproblems:

$$E_{\text{MCE}} = \frac{1}{C} \sum_{i=1}^C E_i, \quad (9)$$

where C is the number of subproblems. The calibration error E_i for the i -th subproblem is defined as the discrepancy between the simulated and observed data within the interval $[\tilde{T}_{\tau_{i-1}}, \tilde{T}_{\tau_i}]$, calculated using the optimal parameters θ_i^* found by the algorithm:

$$E_i = D\left(M(\theta_i^*, \tilde{T}_{\tau_{i-1}}, \tilde{T}_{\tau_i}), \{\hat{s}\}_{\tilde{T}_{\tau_{i-1}}}^{\tilde{T}_{\tau_i}}\right), \quad (10)$$

where $D(\cdot)$ is the discrepancy function, adopting the same formulation as the method of simulated moments in Eq. (8).

2) *Convergence Performance*: To assess the convergence speed and stability, we define the Convergence Performance (P_{CON}) by measuring the average best fitness value across all iterations. Let $F_{i,j}$ denote the best fitness value (i.e., the minimum objective function value found so far) in the j -th iteration of the i -th subproblem. The metric is defined as:

$$P_{\text{CON}} = \frac{1}{C \times N_{\text{iter}}} \sum_{i=1}^C \sum_{j=1}^{N_{\text{iter}}} F_{i,j}, \quad (11)$$

TABLE I: Comparison of subproblem calibration errors (E_i , mean \pm std), mean calibration error (E_{MCE}), and convergence performance (P_{CON} , mean \pm std) across nine benchmark instances (F_1 – F_9) on the Brock–Hommes model. All values are scaled by $\times 10^{-2}$. Bold values indicate the best performance for each metric.

Instance	Error	PosEDO	FBCD-Arch	FBCD-NNIT	FBCD-Rand	DBD-Rand	PosEDO-CD	PosEDO-Pre
F_1	E_1	3.67 \pm 0.14	3.22\pm0.24	3.28 \pm 0.25	3.49 \pm 0.26	4.07 \pm 0.30	3.47 \pm 0.22	4.01 \pm 0.29
	E_2	3.30\pm0.12	4.29 \pm 0.26	4.29 \pm 0.28	4.58 \pm 0.27	5.25 \pm 0.31	4.57 \pm 0.24	4.51 \pm 0.25
	E_3	7.20\pm0.15	10.65 \pm 0.33	9.97 \pm 0.31	12.42 \pm 0.36	10.93 \pm 0.34	8.22 \pm 0.30	8.09 \pm 0.27
	E_{MCE}	4.72	6.05	5.85	6.83	6.75	5.42	5.54
	P_{CON}	5.93\pm0.18	6.52 \pm 0.30	6.69 \pm 0.34	7.74 \pm 0.27	7.12 \pm 0.31	6.48 \pm 0.23	6.61 \pm 0.25
F_2	E_1	4.34\pm0.20	5.22 \pm 0.35	4.85 \pm 0.34	5.95 \pm 0.40	5.56 \pm 0.38	4.50 \pm 0.32	5.01 \pm 0.33
	E_2	4.01 \pm 0.22	4.42 \pm 0.30	3.83\pm0.24	4.87 \pm 0.34	5.73 \pm 0.37	4.54 \pm 0.31	4.32 \pm 0.31
	E_3	10.73\pm0.21	12.18 \pm 0.37	11.94 \pm 0.36	13.25 \pm 0.42	11.99 \pm 0.39	11.25 \pm 0.35	12.45 \pm 0.38
	E_{MCE}	6.36	7.27	6.87	8.02	7.76	6.76	7.26
	P_{CON}	6.52\pm0.23	8.29 \pm 0.21	7.54 \pm 0.33	8.61 \pm 0.32	8.22 \pm 0.26	6.94 \pm 0.19	7.78 \pm 0.26
F_3	E_1	3.45\pm0.15	3.93 \pm 0.27	3.84 \pm 0.27	4.45 \pm 0.30	5.03 \pm 0.33	3.85 \pm 0.28	4.18 \pm 0.28
	E_2	3.11\pm0.14	3.71 \pm 0.27	3.42 \pm 0.26	4.18 \pm 0.31	4.40 \pm 0.35	3.31 \pm 0.26	3.45 \pm 0.27
	E_3	9.61\pm0.16	10.22 \pm 0.31	9.97 \pm 0.30	10.67 \pm 0.33	10.33 \pm 0.32	10.00 \pm 0.31	10.08 \pm 0.30
	E_{MCE}	5.39	5.59	5.74	6.43	6.59	5.72	5.90
	P_{CON}	5.82\pm0.13	6.15 \pm 0.27	6.78 \pm 0.23	6.47 \pm 0.37	6.91 \pm 0.22	6.85 \pm 0.17	6.92 \pm 0.25
F_4	E_1	4.63\pm0.20	9.08 \pm 0.44	4.98 \pm 0.27	17.95 \pm 0.60	5.74 \pm 0.36	4.63\pm0.24	6.82 \pm 0.38
	E_2	5.97 \pm 0.23	6.32 \pm 0.29	6.26 \pm 0.28	7.31 \pm 0.33	5.87\pm0.21	6.02 \pm 0.28	6.26 \pm 0.29
	E_3	6.86\pm0.18	7.02 \pm 0.30	7.09 \pm 0.30	7.16 \pm 0.31	10.58 \pm 0.45	6.93 \pm 0.29	6.92 \pm 0.29
	E_4	5.43 \pm 0.21	8.61 \pm 0.42	5.47 \pm 0.25	5.51 \pm 0.24	6.19 \pm 0.30	5.27\pm0.22	5.31 \pm 0.22
	E_5	8.14 \pm 0.30	7.98 \pm 0.30	7.85\pm0.22	8.05 \pm 0.31	8.65 \pm 0.35	8.38 \pm 0.34	8.13 \pm 0.32
	E_{MCE}	6.21	7.80	6.33	9.20	7.41	6.25	6.69
	P_{CON}	6.77\pm0.07	8.2 \pm 0.19	7.56 \pm 0.32	9.79 \pm 0.23	7.93 \pm 0.25	7.10 \pm 0.19	7.24 \pm 0.33
F_5	E_1	6.93\pm0.14	7.35 \pm 0.28	7.53 \pm 0.29	7.02 \pm 0.26	7.64 \pm 0.31	7.43 \pm 0.29	7.51 \pm 0.29
	E_2	6.78\pm0.12	7.38 \pm 0.27	7.58 \pm 0.30	7.64 \pm 0.29	7.07 \pm 0.26	7.31 \pm 0.27	7.48 \pm 0.28
	E_3	11.82\pm0.20	12.88 \pm 0.39	12.93 \pm 0.39	14.31 \pm 0.43	12.61 \pm 0.37	12.46 \pm 0.36	12.56 \pm 0.37
	E_4	6.47\pm0.11	8.21 \pm 0.34	7.72 \pm 0.30	9.68 \pm 0.41	6.48 \pm 0.25	6.49 \pm 0.25	6.93 \pm 0.27
	E_5	7.24 \pm 0.21	7.28 \pm 0.26	7.22 \pm 0.26	7.48 \pm 0.28	7.67 \pm 0.30	7.20\pm0.23	8.50 \pm 0.45
	E_{MCE}	7.85	8.62	8.60	9.23	8.29	8.18	8.60
	P_{CON}	8.55\pm0.28	9.39 \pm 0.31	9.03 \pm 0.23	9.94 \pm 0.34	8.82 \pm 0.25	8.66 \pm 0.35	9.38 \pm 0.33
F_6	E_1	3.50\pm0.12	3.67 \pm 0.22	3.77 \pm 0.24	3.63 \pm 0.21	4.24 \pm 0.29	3.63 \pm 0.21	3.63 \pm 0.21
	E_2	5.16\pm0.14	5.52 \pm 0.26	5.53 \pm 0.26	5.72\pm0.27	5.41 \pm 0.27	6.05 \pm 0.29	5.59 \pm 0.27
	E_3	10.35\pm0.22	11.92 \pm 0.50	11.38 \pm 0.46	11.54 \pm 0.48	11.11 \pm 0.43	10.72 \pm 0.40	10.48 \pm 0.36
	E_4	8.88 \pm 0.25	9.09 \pm 0.44	12.66 \pm 0.62	14.99 \pm 0.75	7.92 \pm 0.33	7.40\pm0.26	11.20 \pm 0.55
	E_5	10.08\pm0.24	10.24 \pm 0.38	14.46 \pm 0.90	10.85 \pm 0.43	10.39 \pm 0.40	11.21 \pm 0.46	14.41 \pm 0.88
	E_{MCE}	7.59	8.09	9.56	9.35	7.81	7.80	9.06
	P_{CON}	7.92\pm0.13	8.43 \pm 0.24	9.81 \pm 0.19	9.85 \pm 0.26	8.27 \pm 0.30	8.12 \pm 0.18	9.42 \pm 0.23
F_7	E_1	20.38\pm0.28	33.63 \pm 0.55	32.41 \pm 0.52	22.37 \pm 0.40	30.85 \pm 0.50	30.02 \pm 0.48	32.92 \pm 0.54
	E_2	23.72 \pm 0.30	34.84 \pm 0.56	33.96 \pm 0.54	50.91 \pm 0.86	15.62\pm0.22	32.44 \pm 0.50	36.53 \pm 0.62
	E_3	11.85\pm0.20	25.98 \pm 0.61	20.71 \pm 0.48	25.88 \pm 0.60	12.42 \pm 0.31	12.21 \pm 0.30	12.89 \pm 0.33
	E_4	8.66\pm0.18	18.93 \pm 0.57	20.14 \pm 0.62	17.25 \pm 0.52	9.34 \pm 0.24	10.16 \pm 0.26	13.81 \pm 0.38
	E_5	23.20 \pm 0.40	33.25 \pm 0.84	33.52 \pm 0.86	31.45 \pm 0.78	19.16\pm0.30	19.21 \pm 0.42	23.85 \pm 0.52
	E_6	9.34\pm0.18	16.09 \pm 0.58	15.92 \pm 0.56	15.41 \pm 0.55	9.39 \pm 0.24	9.54 \pm 0.24	10.12 \pm 0.28
	E_7	31.78 \pm 0.44	36.24 \pm 0.74	35.33 \pm 0.71	35.19 \pm 0.70	41.54 \pm 0.95	30.62\pm0.48	35.54 \pm 0.72
	E_8	11.87\pm0.22	14.14 \pm 0.36	14.56 \pm 0.37	13.11 \pm 0.32	12.74 \pm 0.30	14.47 \pm 0.34	15.73 \pm 0.42
	E_9	360.90\pm0.90	365.89 \pm 1.22	365.38 \pm 1.22	362.73 \pm 1.20	362.09 \pm 1.18	367.58 \pm 1.25	368.93 \pm 1.28
	E_{MCE}	55.74	64.33	63.55	63.81	57.02	58.47	61.15
F_8	E_1	9.51\pm0.18	10.23 \pm 0.30	9.94 \pm 0.28	11.72 \pm 0.34	12.55 \pm 0.38	12.55 \pm 0.38	12.51 \pm 0.38
	E_2	10.44\pm0.16	11.02 \pm 0.34	10.75 \pm 0.32	12.18 \pm 0.39	11.05 \pm 0.34	10.75 \pm 0.32	11.42 \pm 0.36
	E_3	9.28\pm0.15	10.05 \pm 0.30	9.76 \pm 0.28	10.84 \pm 0.32	14.74 \pm 0.58	10.88 \pm 0.33	10.23 \pm 0.31
	E_4	11.83 \pm 0.31	11.95 \pm 0.38	11.68 \pm 0.37	13.27 \pm 0.46	12.02 \pm 0.40	10.75\pm0.29	11.12 \pm 0.33
	E_5	9.49 \pm 0.24	12.15 \pm 0.52	11.88 \pm 0.49	12.91 \pm 0.60	13.82 \pm 0.72	9.39\pm0.26	10.49 \pm 0.36
	E_6	12.54 \pm 0.32	13.26 \pm 0.48	12.91 \pm 0.46	13.72 \pm 0.52	14.32 \pm 0.62	12.89 \pm 0.44	12.27\pm0.30
	E_7	4.39\pm0.12	6.57 \pm 0.26	5.12 \pm 0.20	5.02 \pm 0.19	4.73 \pm 0.17	5.66 \pm 0.20	5.88 \pm 0.22
	E_8	7.02\pm0.14	9.91 \pm 0.38	9.35 \pm 0.35	9.58 \pm 0.36	9.22 \pm 0.34	7.95 \pm 0.26	8.02 \pm 0.28
	E_9	50.39\pm0.60	84.33 \pm 1.32	83.83 \pm 1.32	74.01 \pm 1.20	87.97 \pm 1.40	52.18 \pm 0.90	53.39 \pm 0.94
	E_{MCE}	13.88	18.83	18.36	18.14	20.05	14.78	15.04
F_9	E_1	4.31 \pm 0.18	5.62 \pm 0.42	5.42 \pm 0.40	5.91 \pm 0.44	4.67 \pm 0.30	4.06\pm0.22	4.07 \pm 0.23
	E_2	5.88\pm0.16	6.12 \pm 0.27	6.01 \pm 0.26	6.43 \pm 0.29	7.29 \pm 0.38	6.65 \pm 0.31	7.02 \pm 0.36
	E_3	9.18 \pm 0.24	11.51 \pm 0.44	12.36 \pm 0.50	10.75 \pm 0.40	9.15\pm0.34	12.11 \pm 0.48	11.44 \pm 0.46
	E_4	5.27\pm0.14	6.54 \pm 0.26	6.41 \pm 0.25	6.84 \pm 0.29	6.80 \pm 0.28	6.80 \pm 0.28	6.65 \pm 0.27
	E_5	19.63 \pm 0.40	19.87 \pm 0.42	19.74 \pm 0.41	20.12 \pm 0.46	19.59 \pm 0.40	19.11\pm0.36	19.35 \pm 0.38
	E_6	11.14\pm0.20	12.93 \pm 0.48	11.82 \pm 0.40	11.22 \pm 0.34	12.08 \pm 0.44	11.85 \pm 0.40	11.90 \pm 0.42
	E_7	21.89\pm0.28	23.08 \pm 0.60	23.97 \pm 0.70	23.39 \pm 0.64	24.80 \pm 0.72	22.00 \pm 0.58	27.60 \pm 0.90
	E_8	29.76 \pm 0.42	30.28 \pm 0.50	34.57 \pm 0.72	32.13 \pm 0.58	30.95 \pm 0.52	29.59\pm0.44	31.92 \pm 0.60
	E_9	16.95\pm0.33	18.27 \pm 0.51	20.18 \pm 0.60	19.66 \pm 0.55	19.81 \pm 0.57	18.04 \pm 0.43	18.13 \pm 0.49
	E_{MCE}	13.78	14.91	15.61	15.16	15.02	14.47	15.34
	P_{CON}	12.97\pm0.38	14.52 \pm 0.31	13.94 \pm 0.42	14.31 \pm 0.42			

where N_{iter} denotes the total number of iterations. A lower P_{CON} indicates that the algorithm discovers better solutions faster and maintains them throughout the process.

To ensure statistical robustness, each instance is executed 10 times under identical experimental settings. The mean and standard deviation of each metric are reported.

D. Experimental Configuration

In the pre-training phase, the dataset D_{pre} used for pre-training, consists of $|\mathcal{D}_{\text{pre}}| = 100000$ training samples. For both the pre-training and fine-tuning configurations, the batch size B is set to 200 and the learning rate η is fixed at 0.0005. The stopping criterion for pretraining is set such that training terminates if the loss does not improve for 20 consecutive iterations, while the fine-tuning stops if the loss shows no improvement for 3 successive iterations. During the change detection process, $N = 2000$ samples are drawn from each posterior distribution for comparison. The KL divergence threshold ε used for change detection is set to 30 for the first simulator and 2 for the second, which we empirically found to provide reliable performance across different test cases. Upon change detection, during the environment adaptation phase, the population size λ for re-initialization is set to 40.

To reduce the influence of randomness, each experiment is independently repeated 10 times under different random seeds. The implementation of AMP/PSO strictly follows the original configuration described in [58], with the number of individuals limited to fewer than 80 and the maximum number of iterations I_{max} set to 10.

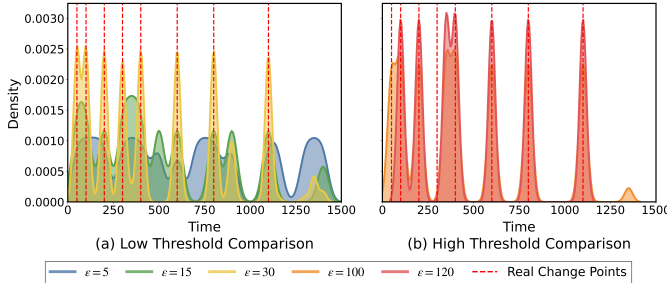


Fig. 2: Change detection accuracy under different thresholds ε on instance F_8 of the Brock–Hommes model. The subplot (a) summarizes low-threshold cases ($\varepsilon = 5, 15, 30$); and subplot (b) shows higher thresholds ($\varepsilon = 100, 120$). Red dashed lines mark the ground-truth change points for comparison.

VI. EXPERIMENTAL RESULTS ON THE ECONOMIC MODEL

This section presents the experimental results of the Brock and Hommes model. We primarily aim to answer: 1) How does our proposed PosEDO method perform compared to traditional EDO methods on simple yet dynamically complex online calibration problems? 2) How accurate is the detection of our proposed method, and how does the detection accuracy impact calibration performance? 3) What is the impact of different change-detection thresholds ε ? 4) How do different environment adaptation mechanisms compare?

TABLE II: Comparison of convergence (P_{CON} , mean \pm std) and calibration (E_{MCE}) results across the 9 instances (F_1 to F_9) on the Brock–Hommes model, assuming perfect change-point detection, to evaluate different environment adaptation strategies. All values are scaled by $\times 10^{-2}$. Bold values indicate the best performance for each metric.

Instance	Metric	Rand	Arch	NNIT	PosEDO-Ada
F_1	P_{CON}	6.34 ± 0.21	6.36 ± 0.29	6.54 ± 0.33	5.89 ± 0.12
	E_{MCE}	5.68	5.78	6.02	4.87
F_2	P_{CON}	6.78 ± 0.25	6.85 ± 0.16	7.08 ± 0.18	6.34 ± 0.09
	E_{MCE}	6.43	6.66	6.36	6.25
F_3	P_{CON}	6.06 ± 0.22	6.92 ± 0.15	6.35 ± 0.41	5.93 ± 0.11
	E_{MCE}	5.59	5.64	6.36	5.24
F_4	P_{CON}	7.25 ± 0.10	7.24 ± 0.17	7.61 ± 0.30	6.70 ± 0.06
	E_{MCE}	6.27	6.08	6.41	6.19
F_5	P_{CON}	8.40 ± 0.11	8.40 ± 0.12	8.78 ± 0.28	8.32 ± 0.21
	E_{MCE}	8.04	7.93	8.14	7.91
F_6	P_{CON}	7.50 ± 0.25	7.95 ± 0.23	7.54 ± 0.10	7.38 ± 0.09
	E_{MCE}	7.31	7.70	7.28	7.24
F_7	P_{CON}	13.95 ± 0.13	15.01 ± 0.14	14.92 ± 0.16	13.71 ± 0.10
	E_{MCE}	59.58	63.66	63.82	57.21
F_8	P_{CON}	17.92 ± 0.30	19.95 ± 0.43	18.21 ± 0.38	15.54 ± 0.24
	E_{MCE}	15.12	18.24	16.15	13.98
F_9	P_{CON}	14.45 ± 0.36	14.63 ± 0.26	14.55 ± 0.31	13.21 ± 0.33
	E_{MCE}	20.71	20.75	21.73	19.82

A. The Overall Performance

To answer the first question, we provide a comprehensive evaluation of the calibration (E_{MCE}) and convergence performance (P_{CON}) of all seven compared algorithms across nine benchmark instances (F_1 – F_9) in Table I. Furthermore, a granular analysis is conducted to examine the calibration error within each subproblem (e.g., E_1, E_2, \dots) of these instances.

Compared with traditional EDO methods, our proposed PosEDO achieves the best performance across most instances, including calibration error per subproblem, overall average calibration error, and convergence across the entire instance. This indicates that the posterior distribution-assisted change detection and environment adaptation mechanisms in PosEDO are more capable of detecting system changes and effectively exploring new environments, further validating the limitations of traditional methods for this type of DOP. From the table, it is also notable that there are significant numerical variations across different instances, and the error values for specific subproblems are particularly high (e.g., E_9 in F_8). This is attributed to search space constraints, which prevented the algorithm from finding more suitable parameters.

Regarding the specific components, by utilizing identical environment adaptation strategies but different change detection methods, PosEDO-CD consistently outperforms DBD-Rand and FBCD-Rand across most instances. This superiority validates that embedding posterior knowledge into the change detection mechanism yields more precise calibration outcomes than conventional detection heuristics. Furthermore, PosEDO-Pre, which relies exclusively on a static pretrained posterior without online fine-tuning, exhibits markedly inferior performance compared to the complete PosEDO framework. This pronounced discrepancy underscores the indispensability of continuous posterior refinement to maintain long-term calibration stability in dynamic environments.

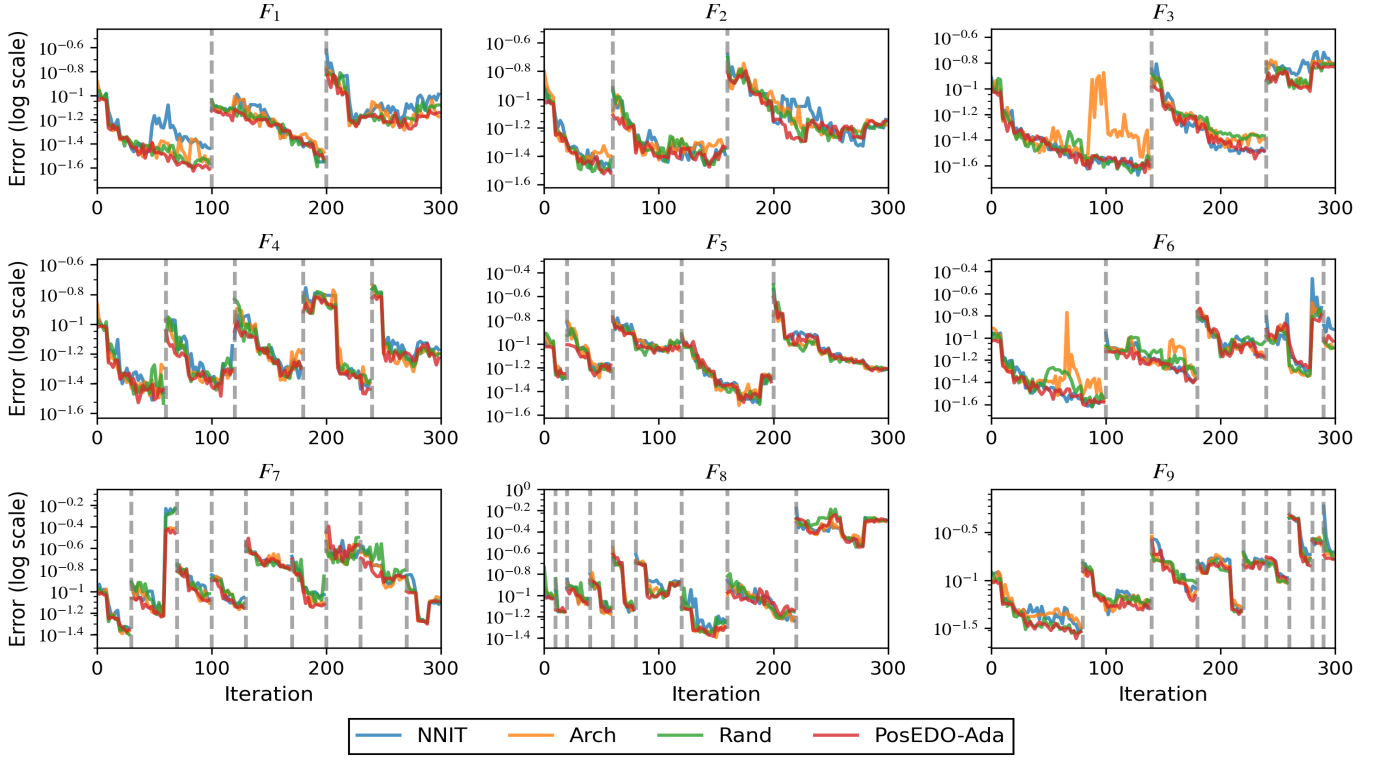


Fig. 3: Under the assumption that the change points are correctly detected, the calibration error comparison of NNIT, Arch, Rand, and PosEDO-Ada across 9 instances (F_1 – F_9) on the Brock–Hommes model. The horizontal axis represents the iterations, and the vertical axis represents the error value in log scale. And the vertical dashed lines indicate the true changes.

B. Change Detection

In the overall calibration results presented in Table I, the PosEDO-CD consistently performs better than both DBD-Rand and FBCD-Rand. Since these three methods share the same optimization and environment adaptation mechanisms and differ only in their change detection strategies, their performance gap implies that the quality of detected change points is crucial for achieving accurate online calibration.

To further investigate this relationship, we performed a statistical analysis of the change points detected by these three methods during the online calibration process. For each method, the detections from 10 independent runs are aggregated and converted into probability density functions via kernel density estimation. Subsequently, these estimated densities are compared against the ground-truth change points (indicated by red dashed lines), as illustrated in Fig. 1.

Across all instances with change frequencies ranging from low to high, the proposed PosEDO-CD exhibits concentrated density peaks closely aligned with the true change points. This indicates that the posterior-assisted change detector yields highly consistent detection signals over repeated runs that correspond accurately to the ground truth. In contrast, the density curves of the DBD method are noticeably more dispersed and exhibit frequent false alarms. This occurs because detectors placed at fixed locations experience fluctuations in their fitness values upon the arrival of new observations, which are then misinterpreted as true parameter changes. Comparatively, FBCD produces fewer false alarms than DBD, yet

its detections remain inaccurate. These phenomena are fully consistent with our earlier discussion regarding the limitations of fitness-based detection methods.

Therefore, these observations provide a clear explanation for the relative performance of the three change detection methods reported in Table I. Since the proposed PosEDO-CD detects change points with greater reliability, its optimization process is able to respond to environmental changes more promptly than DBD-Rand and FBCD-Rand, thereby achieving superior calibration performance. Consequently, the delayed or unstable detections of the baseline methods lead to outdated or inappropriate search states, ultimately resulting in inferior calibration performance.

C. Different Change Detection Thresholds ϵ

To investigate the sensitivity of detection accuracy to the change detection threshold ϵ , we evaluated the performance of our method across the settings $\epsilon \in \{5, 15, 30, 100, 120\}$. For each setting, we similarly aggregated the detected change points from 10 independent runs to construct probability density functions via kernel density estimation, comparing them against the true change points. The results show that the detection accuracy reaches its peak when ϵ is around 30.

To demonstrate the impact of different threshold values, Fig. 2 illustrates the results on instance F_8 . Specifically, Fig. 2(a) shows the results when $\epsilon \leq 30$, while Fig. 2(b) presents the case where $\epsilon > 30$. It can be observed that when the threshold is very small (e.g., $\epsilon = 5$), the detector

TABLE III: Comparison of subproblem calibration errors (E_i , mean \pm std), mean calibration error (E_{MCE}), and convergence performance (P_{CON} , mean \pm std) across 9 benchmark instances (F_1 – F_9) on the PGPS model. Bold values indicate the best performance for each metric.

Instance	Subproblem	PosEDO-CD	DBD-Rand	FBCD-Rand	FBCD-Arch	FBCD-NNIT	PosEDO
F_1	E_1	6.38 \pm 2.19	7.85 \pm 1.97	7.37 \pm 3.62	6.40 \pm 1.92	6.02 \pm 1.87	5.37\pm1.48
	E_2	16.57 \pm 5.82	85.46 \pm 30.43	37.22 \pm 28.33	80.72 \pm 44.28	62.97 \pm 39.12	12.18\pm3.31
	E_3	41.26 \pm 8.63	76.71 \pm 34.88	75.44 \pm 26.79	96.90 \pm 64.31	73.11 \pm 49.71	40.70\pm9.27
	E_{MCE}	21.40	56.67	40.01	61.34	47.37	19.42
	P_{CON}	23.15 \pm 4.55	60.22 \pm 15.30	43.10 \pm 9.80	65.40 \pm 18.12	50.85 \pm 12.44	21.15\pm3.25
F_2	E_1	2.86 \pm 1.12	8.14 \pm 2.46	2.03 \pm 1.01	1.59\pm0.04	2.07 \pm 0.93	2.37 \pm 1.33
	E_2	18.47 \pm 6.18	92.36 \pm 27.41	28.31 \pm 24.25	50.34 \pm 18.87	25.33 \pm 10.13	14.53\pm4.96
	E_3	16.37 \pm 9.85	81.44 \pm 35.22	20.30 \pm 8.39	74.97 \pm 68.25	36.91 \pm 26.79	14.06\pm10.12
	E_{MCE}	12.57	60.65	16.88	42.30	21.44	10.32
	P_{CON}	13.92 \pm 3.10	64.12 \pm 22.45	18.25 \pm 5.12	45.80 \pm 14.20	23.55 \pm 7.60	11.88\pm2.62
F_3	E_1	5.92 \pm 1.35	7.93 \pm 2.14	5.14 \pm 1.66	5.14 \pm 1.26	5.03 \pm 1.22	4.93\pm1.42
	E_2	20.80\pm7.30	55.31 \pm 16.14	21.20 \pm 8.30	49.74 \pm 15.66	51.79 \pm 31.33	20.97 \pm 7.50
	E_3	4.36 \pm 1.47	4.08 \pm 1.79	3.92 \pm 1.20	3.39 \pm 1.71	3.28\pm1.82	3.90 \pm 3.32
	E_{MCE}	10.36	22.44	10.09	19.42	20.03	9.93
	P_{CON}	12.12 \pm 2.45	24.50 \pm 6.22	10.85\pm1.78	21.10 \pm 5.45	22.40 \pm 7.88	11.02 \pm 2.15
F_4	E_1	4.95\pm1.38	8.47 \pm 2.34	6.12 \pm 1.88	6.05 \pm 1.74	5.84 \pm 1.63	5.12 \pm 1.45
	E_2	24.13 \pm 7.41	61.37 \pm 20.58	27.95 \pm 11.33	76.20 \pm 30.10	29.41 \pm 13.02	22.10\pm6.88
	E_3	3.83 \pm 1.33	4.67 \pm 1.97	3.62 \pm 1.48	3.55 \pm 1.60	3.08\pm1.18	3.45 \pm 1.25
	E_4	9.87 \pm 2.81	17.80 \pm 6.10	10.92 \pm 3.01	11.37 \pm 3.26	10.44 \pm 2.77	9.18\pm2.32
	E_{MCE}	10.70	23.08	12.15	24.29	12.19	9.96
F_5	E_1	6.55\pm1.65	13.85 \pm 4.10	8.35 \pm 2.44	7.80 \pm 2.20	7.31 \pm 2.01	6.72 \pm 1.74
	E_2	14.47 \pm 4.41	31.80 \pm 10.20	12.90 \pm 5.22	11.72\pm4.05	13.22 \pm 5.01	12.02 \pm 4.12
	E_3	4.07 \pm 1.23	6.36 \pm 2.03	4.61 \pm 1.58	4.20 \pm 1.40	4.11 \pm 1.36	3.74\pm1.14
	E_4	10.23 \pm 3.07	20.40 \pm 6.60	11.62 \pm 3.48	11.10 \pm 3.20	10.92 \pm 3.06	9.80\pm2.76
	E_{MCE}	8.83	18.10	9.37	8.71	8.89	8.07
F_6	E_1	5.74 \pm 1.64	9.47 \pm 2.68	6.85 \pm 1.98	6.30 \pm 1.88	6.12 \pm 1.79	5.52\pm1.58
	E_2	25.13 \pm 6.33	48.78 \pm 15.42	23.44 \pm 9.60	58.40 \pm 23.10	22.30 \pm 8.80	19.80\pm5.88
	E_3	3.55 \pm 1.18	5.12 \pm 1.74	3.72 \pm 1.26	3.40 \pm 1.22	3.10\pm1.04	3.28 \pm 1.10
	E_4	8.08\pm2.18	14.57 \pm 4.82	9.12 \pm 2.66	9.05 \pm 2.62	8.92 \pm 2.58	8.63 \pm 2.46
	E_{MCE}	10.63	19.49	10.78	19.29	10.11	9.31
F_7	E_1	12.18 \pm 2.65	21.80 \pm 6.88	12.33 \pm 3.22	22.15 \pm 7.40	11.75 \pm 2.92	10.88\pm2.08
	E_2	5.33 \pm 1.55	9.05 \pm 2.55	5.92 \pm 1.78	5.70 \pm 1.66	5.48 \pm 1.60	5.02\pm1.41
	E_3	16.87 \pm 5.41	42.10 \pm 14.30	18.44 \pm 7.30	17.92 \pm 6.85	17.40 \pm 6.44	15.48\pm5.06
	E_4	3.22 \pm 1.02	4.88 \pm 1.66	3.48 \pm 1.18	3.02\pm0.96	3.30 \pm 1.10	3.12 \pm 1.00
	E_5	12.47 \pm 3.12	22.50 \pm 7.60	12.30 \pm 3.44	12.12 \pm 3.38	11.92 \pm 3.22	10.78\pm2.88
F_8	E_1	7.88 \pm 2.22	13.47 \pm 4.23	8.44 \pm 2.35	8.22 \pm 2.30	8.10 \pm 2.25	7.36\pm2.02
	E_2	9.15	18.40	9.72	9.40	9.24	8.35
	E_3	10.65 \pm 2.33	21.22 \pm 6.40	11.20 \pm 3.05	10.95 \pm 2.88	10.82 \pm 2.75	9.78\pm2.02
	E_4	4.92 \pm 1.41	7.83 \pm 2.22	5.22 \pm 1.67	5.05 \pm 1.55	4.98 \pm 1.50	4.60\pm1.34
	E_5	18.24 \pm 6.07	41.53 \pm 13.43	25.60 \pm 9.80	22.40 \pm 8.20	19.05 \pm 7.20	17.32\pm5.64
F_9	E_1	3.55 \pm 1.12	4.92 \pm 1.70	3.70 \pm 1.28	3.40 \pm 1.08	3.35 \pm 1.06	3.16\pm1.02
	E_2	10.47 \pm 3.03	19.24 \pm 6.41	11.05 \pm 3.20	9.92\pm2.86	10.12 \pm 2.95	10.10 \pm 2.92
	E_3	6.64 \pm 1.93	12.47 \pm 3.89	7.05 \pm 2.02	6.90 \pm 1.98	6.80 \pm 1.95	6.28\pm1.78
	E_4	8.76	17.20	10.52	9.53	8.86	8.29
	E_{MCE}	9.35\pm2.15	19.80 \pm 5.92	12.15 \pm 3.44	11.20 \pm 3.02	10.10 \pm 1.95	9.62 \pm 1.88

becomes overly sensitive, leading to frequent false alarms, as it is more prone to detecting minute variations. In contrast, when the threshold is too large (e.g., $\varepsilon = 100$ or 120), detections are often delayed in capturing true changes, thereby favoring the detection of only significant shifts. When the threshold is set around $\varepsilon = 30$, the estimated detection probability densities align closely with the ground-truth change points. These results demonstrate that a moderate threshold is crucial for balancing sensitivity and robustness, thereby achieving more accurate and stable change detection.

D. Environment Adaptation

In this subsection, we aim to directly investigate the effect of different environment adaptation strategies on algorithmic convergence and calibration performance. To isolate the effect of environment adaptation, four strategies are considered: Rand, Arch, NNIT, and our proposed environment adaptation method (PosEDO-Ada), under the assumption that the change points are correctly detected. The results across the nine instances are summarized in Table II.

Overall, PosEDO-Ada achieves the best convergence performance across all instances and consistently yields the smallest

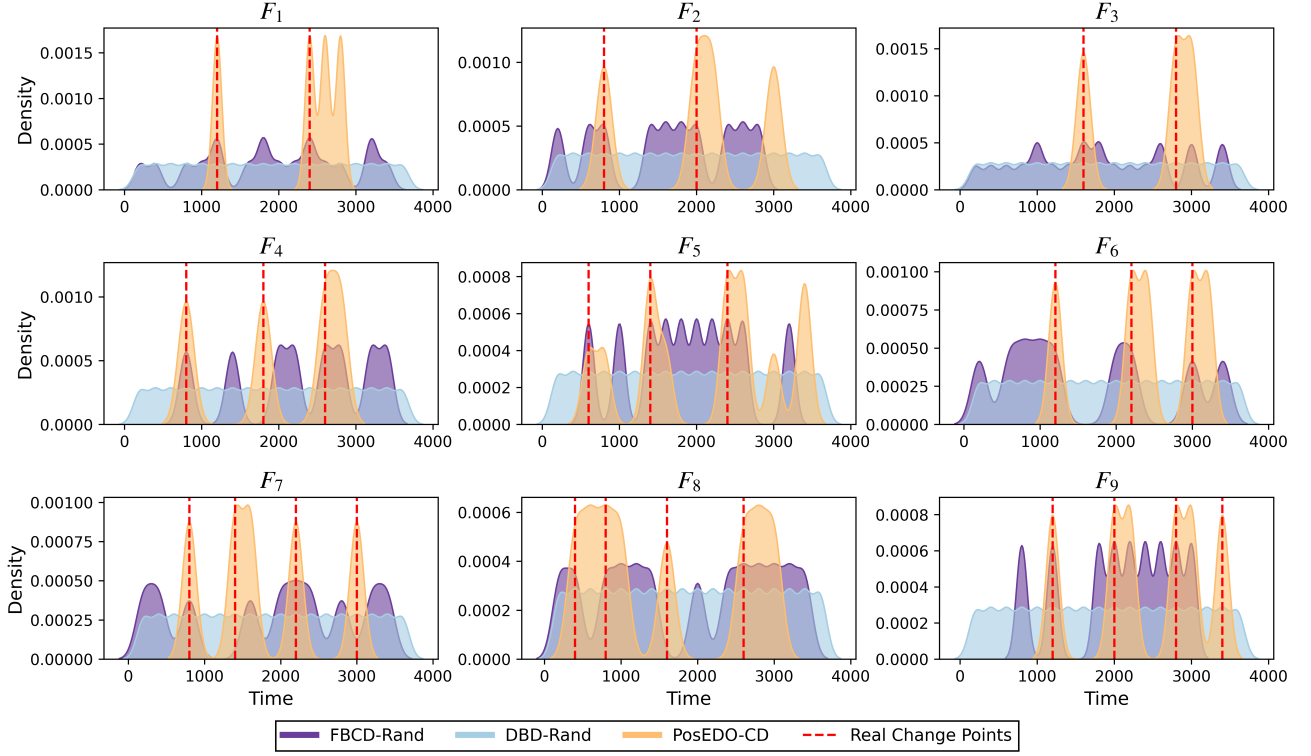


Fig. 4: Detection accuracy comparison across 9 problem instances (F_1 – F_9) on the PGPS model. In each subplot, the red dashed lines indicate the ground-truth change times. The purple, blue, and orange curves represent the change detection probability densities of FBCD-Rand, DBD-Rand, and PosEDO-CD, respectively.

calibration error in nearly every case. This indicates that by leveraging posterior estimation, PosEDO-Ada effectively guides the population to search for superior regions. Fig. 3 illustrates the convergence curves of the calibration error for the four algorithms over the course of iterations, where vertical dashed lines indicate the moments of environmental changes. It can be observed that the PosEDO-Ada consistently remains below the other three methods in most instances, demonstrating superior convergence and calibration performance. Furthermore, the PosEDO-Ada exhibits smaller errors in the new environments immediately following changes, indicating that the posterior distribution of parameters provides better initial conditions for the new environment. In the online calibration process, since the variations in the parameter space do not exhibit smooth moving peaks or periodic changes, the Arch and NNIT methods fail to effectively guide the exploration of the algorithms in the new environment. Moreover, they may even mislead the search process toward inferior regions. Notably, as observational data accumulates, the calibration error fluctuates continuously during the iterations within subproblems due to the data influence; in particular, the arrival of new data may induce drastic fluctuations in the calibration error.

VII. EXPERIMENTAL RESULTS ON THE FINANCIAL MODEL

This section presents the experimental results of PosEDO on the PGPS model. Compared with the Brock–Hommes simulator, the PGPS environment features higher parameter

dimensionality and a more intricate micro-level price formation mechanism, making online calibration substantially more challenging. Table III reports the calibration and convergence performance of six algorithms (excluding PosEDO-Pre) across nine PGPS instances (F_1 – F_9). Across nearly all instances and subproblems, PosEDO achieves the best performance among all compared methods, demonstrating strong advantages in both estimation accuracy and convergence stability. However, compared with the results on the Brock–Hommes instances, a performance degradation is evident in terms of both convergence and calibration accuracy. This is attributed to the multi-parameter interactions and richer non-linear market dynamics in these instances, which significantly increase the difficulty of the optimization task.

Fig. 4 illustrates the change detection results of PosEDO-CD, DBD-Rand, and FBCD-Rand on the PGPS model. Overall, the detections produced by PosEDO remain sharply concentrated around the ground-truth change points, demonstrating that the posterior-based detector is still able to provide accurate and stable signals in this substantially more complex environment. However, compared with the results on the Brock–Hommes model, while PosEDO is equally capable of detecting system environmental changes, it also exhibits a higher number of false detections. This indicates that although the detector captures the true changes, the increased stochasticity and micro-level fluctuations in the PGPS simulator make the posterior more sensitive, leading to false alarms. By contrast, both DBD-Rand and FBCD-Rand continue to

perform poorly under the PGPS setting. DBD-Rand suffers from severe false alarms due to fitness fluctuations at each new observation, while FBCD-Rand frequently produces delayed or misaligned peaks, as the fitness trajectory remains an unreliable indicator of environmental shifts in such a high-dimensional and interaction-rich system.

Overall, the experimental results confirm that PosEDO remains effective even within the intricate PGPS environment. While the complex market dynamics pose significant hurdles for baseline algorithms, PosEDO successfully leverages its posterior estimation to achieve precise calibration and change detection. This attests to the method's potential for solving online calibration problems in complex social systems where traditional strategies fail.

VIII. CONCLUSIONS AND FUTURE WORKS

This paper investigates the online calibration problems of complex social simulators by formulating it as DOPs, thereby extending EDO to a broader range of applications. We first explore the limitations of existing EDO methods in handling environmental changes triggered by continuous data streams. To address these challenges, we propose the PosEDO framework, which bridges the critical gap between the parameter and data spaces by explicitly modeling the posterior distribution of parameters. Regarding implementation, by utilizing an MAF model, the PosEDO achieves robust change detection via KL divergence and significantly accelerates environment adaptation through posterior-guided sampling. Calibration experiments conducted on 18 instances across two distinct simulators demonstrate that PosEDO significantly outperforms traditional EDO baselines in terms of both calibration accuracy and convergence stability.

Despite that the proposed PosEDO mainly studied the calibration problem in this work, we think the general idea of learning posterior of data stream and model parameter can be generally applicable to more widely online data stream driven optimization problems, e.g., online learning and online symbolic regression. We will investigate them in the future.

ACKNOWLEDGMENT

This work was supported in part by the National Natural Science Foundation of China under Grant 62272210 and Grant 62331014, and in part by the Zhongguancun Academy under Grant 02012403.

REFERENCES

- [1] J. D. Farmer and D. Foley, "The economy needs agent-based modelling," *Nature*, vol. 460, no. 7256, pp. 685–686, 2009.
- [2] W. A. Brock and C. H. Hommes, "Heterogeneous beliefs and routes to chaos in a simple asset pricing model," *Journal of Economic Dynamics and Control*, vol. 22, no. 8-9, pp. 1235–1274, 1998.
- [3] P. Belcak, J.-P. Calliess, and S. Zohren, "Fast agent-based simulation framework of limit order books with applications to pro-rata markets and the study of latency effects," *CoRR*, 2020.
- [4] D. Byrd, M. Hybinette, and T. H. Balch, "Abides: Towards high-fidelity multi-agent market simulation," in *Proceedings of the 2020 ACM SIGSIM Conference on Principles of Advanced Discrete Simulation*, 2020, pp. 11–22.
- [5] N. M. Ferguson, D. A. Cummings, S. Cauchemez, C. Fraser, S. Riley, A. Meeyai, S. Iamsirithaworn, and D. S. Burke, "Strategies for containing an emerging influenza pandemic in southeast asia," *Nature*, vol. 437, no. 7056, pp. 209–214, 2005.
- [6] N. Oreskes, K. Shrader-Frechette, and K. Belitz, "Verification, validation, and confirmation of numerical models in the earth sciences," *Science*, vol. 263, no. 5147, pp. 641–646, 1994.
- [7] R. G. Sargent, "Verification and validation of simulation models," in *Proceedings of the 2010 winter simulation conference*. IEEE, 2010, pp. 166–183.
- [8] J. Grazzini and M. Richiardi, "Estimation of ergodic agent-based models by simulated minimum distance," *Journal of Economic Dynamics and Control*, vol. 51, pp. 148–165, 2015.
- [9] D. Platt, "A comparison of economic agent-based model calibration methods," *Journal of Economic Dynamics and Control*, vol. 113, p. 103859, 2020.
- [10] J. Kennedy and R. Eberhart, "Particle swarm optimization," in *Proceedings of ICNN'95-international conference on neural networks*, vol. 4. ieee, 1995, pp. 1942–1948.
- [11] R. Storn and K. Price, "Differential evolution—a simple and efficient heuristic for global optimization over continuous spaces," *Journal of global optimization*, vol. 11, no. 4, pp. 341–359, 1997.
- [12] J. Zhao, C. Zhang, M. Qin, and P. Yang, "Quantfactor reinforce: mining steady formulae alpha factors with variance-bounded reinforce," *IEEE Transactions on Signal Processing*, 2025.
- [13] Z. Yang, M. Zhong, and P. Yang, "Evolutionary dynamic optimization-based calibration framework for agent-based financial market simulators," in *2024 IEEE Congress on Evolutionary Computation (CEC)*. IEEE, 2024, pp. 01–08.
- [14] D. Kim, T.-S. Yun, I.-C. Moon, and J. W. Bae, "Automatic calibration of dynamic and heterogeneous parameters in agent-based models," *Autonomous Agents and Multi-Agent Systems*, vol. 35, no. 2, p. 46, 2021.
- [15] J. A. Ward, A. J. Evans, and N. S. Malleson, "Dynamic calibration of agent-based models using data assimilation," *Royal Society open science*, vol. 3, no. 4, p. 150703, 2016.
- [16] A. Carrassi, M. Bocquet, L. Bertino, and G. Evensen, "Data assimilation in the geosciences: An overview of methods, issues, and perspectives," *Wiley Interdisciplinary Reviews: Climate Change*, vol. 9, no. 5, p. e535, 2018.
- [17] T. T. Nguyen, S. Yang, and J. Branke, "Evolutionary dynamic optimization: A survey of the state of the art," *Swarm and Evolutionary Computation*, vol. 6, pp. 1–24, 2012.
- [18] T. T. Nguyen and X. Yao, "Continuous dynamic constrained optimization—the challenges," *IEEE Transactions on Evolutionary Computation*, vol. 16, no. 6, pp. 769–786, 2012.
- [19] D. Yazdani, W. Luo, and S. Yang, "Guest editorial evolutionary dynamic optimization," *IEEE Transactions on Evolutionary Computation*, vol. 29, no. 5, pp. 1458–1462, 2025.
- [20] J. Branke, "Memory enhanced evolutionary algorithms for changing optimization problems," in *Proceedings of the 1999 Congress on Evolutionary Computation-CEC99 (Cat. No. 99TH8406)*, vol. 3. IEEE, 1999, pp. 1875–1882.
- [21] X. Hu and R. C. Eberhart, "Adaptive particle swarm optimization: detection and response to dynamic systems," in *Proceedings of the 2002 congress on evolutionary computation. CEC'02 (cat. No. 02TH8600)*, vol. 2. IEEE, 2002, pp. 1666–1670.
- [22] D. Yazdani, R. Cheng, D. Yazdani, J. Branke, Y. Jin, and X. Yao, "A survey of evolutionary continuous dynamic optimization over two decades—part a," *IEEE Transactions on Evolutionary Computation*, vol. 25, no. 4, pp. 609–629, 2021.
- [23] ———, "A survey of evolutionary continuous dynamic optimization over two decades—part b," *IEEE Transactions on Evolutionary Computation*, vol. 25, no. 4, pp. 630–650, 2021.
- [24] S. Yang and X. Yao, "Population-based incremental learning with associative memory for dynamic environments," *IEEE Transactions on evolutionary computation*, vol. 12, no. 5, pp. 542–561, 2008.
- [25] ———, "Population-based incremental learning with associative memory for dynamic environments," *IEEE Transactions on evolutionary computation*, vol. 12, no. 5, pp. 542–561, 2008.
- [26] J. Branke, *Evolutionary optimization in dynamic environments*. Springer Science & Business Media, 2012, vol. 3.
- [27] Y. Wang and B. Li, "Investigation of memory-based multi-objective optimization evolutionary algorithm in dynamic environment," in *2009 IEEE Congress on Evolutionary Computation*. IEEE, 2009, pp. 630–637.

[28] G. Papamakarios and I. Murray, "Fast ϵ -free inference of simulation models with bayesian conditional density estimation," *Advances in neural information processing systems*, vol. 29, 2016.

[29] T. Ma and B. Abdulhai, "Genetic algorithm-based optimization approach and generic tool for calibrating traffic microscopic simulation parameters," *Transportation research record*, vol. 1800, no. 1, pp. 6–15, 2002.

[30] A. Delaunoy, J. Hermans, F. Rozet, A. Wehenkel, and G. Louppe, "Towards reliable simulation-based inference with balanced neural ratio estimation," *Advances in Neural Information Processing Systems*, vol. 35, pp. 20 025–20 037, 2022.

[31] M. A. Beaumont, W. Zhang, and D. J. Balding, "Approximate bayesian computation in population genetics," *Genetics*, vol. 162, no. 4, pp. 2025–2035, 2002.

[32] J.-M. Lueckmann, P. J. Goncalves, G. Bassetto, K. Öcal, M. Nonnenmacher, and J. H. Macke, "Flexible statistical inference for mechanistic models of neural dynamics," *Advances in neural information processing systems*, vol. 30, 2017.

[33] D. Greenberg, M. Nonnenmacher, and J. Macke, "Automatic posterior transformation for likelihood-free inference," in *International conference on machine learning*. PMLR, 2019, pp. 2404–2414.

[34] D. McFadden, "A method of simulated moments for estimation of discrete response models without numerical integration," *Econometrica: Journal of the Econometric Society*, pp. 995–1026, 1989.

[35] Y. Li, Y. Wu, M. Zhong, S. Liu, and P. Yang, "Simlob: Learning representations of limited order book for financial market simulation," *arXiv preprint arXiv:2406.19396*, 2024.

[36] E. Bernton, P. E. Jacob, M. Gerber, and C. P. Robert, "On parameter estimation with the wasserstein distance," *Information and Inference: A Journal of the IMA*, vol. 8, no. 4, pp. 657–676, 2019.

[37] Y. Bai, H. Lam, T. Balch, and S. Vyetrenko, "Efficient calibration of multi-agent simulation models from output series with bayesian optimization," in *Proceedings of the Third ACM International Conference on AI in Finance*, 2022, pp. 437–445.

[38] C. Wang, J. Ren, and P. Yang, "Alleviating nonidentifiability: a high-fidelity calibration objective for financial market simulation with multivariate time series data," *IEEE Transactions on Computational Social Systems*, 2025.

[39] T. Schnier and X. Yao, "Evolutionary design calibration," in *International Conference on Evolvable Systems*. Springer, 2001, pp. 26–37.

[40] X. Yu, Y. Wang, L. Zhu, D. Filev, and X. Yao, "Engine calibration with surrogate-assisted bilevel evolutionary algorithm," *IEEE Transactions on Cybernetics*, vol. 54, no. 6, pp. 3832–3845, 2023.

[41] J. Zhu, Y. Yao, W. Tang, and H. Zhang, "Dynamic parameter calibration framework for opinion dynamics models," *Entropy*, vol. 24, no. 8, p. 1112, 2022.

[42] Y. Zhang, B. Atasoy, A. Akkinepally, and M. Ben-Akiva, "Dynamic toll pricing using dynamic traffic assignment system with online calibration," *Transportation Research Record*, vol. 2673, no. 10, pp. 532–546, 2019.

[43] A. Carlisle and G. Dozler, "Tracking changing extrema with adaptive particle swarm optimizer," in *Proceedings of the 5th biannual world automation congress*, vol. 13. IEEE, 2002, pp. 265–270.

[44] X. Hu and R. C. Eberhart, "Adaptive particle swarm optimization: detection and response to dynamic systems," in *Proceedings of the 2002 congress on evolutionary computation. CEC'02 (cat. No. 02TH8600)*, vol. 2. IEEE, 2002, pp. 1666–1670.

[45] Y. G. Woldesenbet and G. G. Yen, "Dynamic evolutionary algorithm with variable relocation," *IEEE Transactions on Evolutionary Computation*, vol. 13, no. 3, pp. 500–513, 2009.

[46] X.-F. Liu, Z.-H. Zhan, T.-L. Gu, S. Kwong, Z. Lu, H. B.-L. Duh, and J. Zhang, "Neural network-based information transfer for dynamic optimization," *IEEE transactions on neural networks and learning systems*, vol. 31, no. 5, pp. 1557–1570, 2019.

[47] X.-F. Liu, Z.-H. Zhan, and J. Zhang, "Neural network for change direction prediction in dynamic optimization," *IEEE access*, vol. 6, pp. 72 649–72 662, 2018.

[48] P. D. Stroud, "Kalman-extended genetic algorithm for search in nonstationary environments with noisy fitness evaluations," *IEEE Transactions on Evolutionary Computation*, vol. 5, no. 1, pp. 66–77, 2002.

[49] K. Li, R. Chen, and X. Yao, "A data-driven evolutionary transfer optimization for expensive problems in dynamic environments," *IEEE Transactions on Evolutionary Computation*, 2023.

[50] F. Wang, J. Xie, A. Zhou, and K. Tang, "A new prediction strategy for dynamic multi-objective optimization using diffusion model," *IEEE Transactions on Evolutionary Computation*, 2025.

[51] Y. Hu, J. Ou, P. N. Suganthan, W. Pedrycz, R. Wang, J. Zheng, J. Zou, and Y. Song, "Dynamic multi-objective optimization algorithm guided by recurrent neural network," *management*, vol. 5, p. 6, 2024.

[52] M. C. Du Plessis and A. P. Engelbrecht, "Differential evolution for dynamic environments with unknown numbers of optima," *Journal of Global Optimization*, vol. 55, no. 1, pp. 73–99, 2013.

[53] D. Yazdani, B. Nasiri, A. Sepas-Moghaddam, and M. R. Meybodi, "A novel multi-swarm algorithm for optimization in dynamic environments based on particle swarm optimization," *Applied Soft Computing*, vol. 13, no. 4, pp. 2144–2158, 2013.

[54] C. Li, T. T. Nguyen, M. Yang, S. Yang, and S. Zeng, "Multi-population methods in unconstrained continuous dynamic environments: The challenges," *Information Sciences*, vol. 296, pp. 95–118, 2015.

[55] P. Yang, J. Ren, F. Wang, and K. Tang, "Towards calibrating financial market simulators with high-frequency data," *Complex System Modeling and Simulation*, 2025.

[56] T. Preis, S. Golke, W. Paul, and J. J. Schneider, "Multi-agent-based order book model of financial markets," *Europhysics Letters*, vol. 75, no. 3, p. 510, 2006.

[57] K. Goosen, "Calibrating high frequency trading data to agent based models using approximate bayesian computation," 2021.

[58] C. Li, T. T. Nguyen, M. Yang, M. Mavrovouniotis, and S. Yang, "An adaptive multipopulation framework for locating and tracking multiple optima," *IEEE transactions on evolutionary computation*, vol. 20, no. 4, pp. 590–605, 2015.